PP2A^{Rts1} is a master regulator of pathways that control cell size

Jessica Zapata,[1] Noah Dephoure,[2] Tracy MacDonough,[1] Yaxin Yu,[3] Emily J. Parnell,[3] Meghan Mooring,[1] Steven P. Gygi,[2] David J. Stillman,[3] and Douglas R. Kellogg[1]

[1]Department of Molecular, Cell and Developmental Biology, University of California, Santa Cruz, Santa Cruz, CA 95064
[2]Department of Cell Biology, Harvard Medical School, Boston, MA 02115
[3]Department of Pathology, University of Utah Health Sciences Center, Salt Lake City, UT 84112

Cell size checkpoints ensure that passage through G1 and mitosis occurs only when sufficient growth has occurred. The mechanisms by which these checkpoints work are largely unknown. PP2A associated with the Rts1 regulatory subunit (PP2A^{Rts1}) is required for cell size control in budding yeast, but the relevant targets are unknown. In this paper, we used quantitative proteome-wide mass spectrometry to identify proteins controlled by PP2A^{Rts1}. This revealed that PP2A^{Rts1} controls the two key checkpoint pathways thought to regulate the cell cycle in response to cell growth. To investigate the role of PP2A^{Rts1} in these pathways, we focused on the Ace2 transcription factor, which is thought to delay cell cycle entry by repressing transcription of the G1 cyclin *CLN3*. Diverse experiments suggest that PP2A^{Rts1} promotes cell cycle entry by inhibiting the repressor functions of Ace2. We hypothesize that control of Ace2 by PP2A^{Rts1} plays a role in mechanisms that link G1 cyclin accumulation to cell growth.

Introduction

Cell size must be tightly controlled to ensure function and survival (Jorgensen and Tyers, 2004; Turner et al., 2012). Control of cell size in dividing cells is achieved via cell size checkpoints, which delay key cell cycle transitions until sufficient growth has occurred. Despite their name, it is uncertain whether cell size checkpoints monitor a parameter linked to cell size, such as volume or surface area, or whether they monitor parameters linked to growth or biosynthetic capacity. Discovery of checkpoint signals that link the cell cycle to cell growth is thus an essential step toward understanding how cell size is controlled.

Cell size checkpoints operate at entry into the cell cycle in G1 and again at mitosis. The mitotic checkpoint works through the Wee1 kinase, which delays mitosis via inhibitory phosphorylation of Cdk1 (Nurse, 1975; Gould and Nurse, 1989). Wee1 is a dose-dependent regulator of cell size. Thus, loss of Wee1 in fission yeast causes premature entry into mitosis at a reduced cell size, whereas increased activity of Wee1 causes delayed entry into mitosis and increased cell size (Nurse, 1975; Russell and Nurse, 1987). The signals that connect Cdk1 inhibitory phosphorylation to cell growth are poorly understood.

The G1 cell size checkpoint is best understood in budding yeast. Cell division in budding yeast is asymmetric, yielding a large mother cell and a small daughter cell. The observation that the small daughter cell spends more time undergoing growth in G1 provided early evidence for the existence of cell size checkpoints (Hartwell and Unger, 1977; Johnston et al., 1977). It also focused attention on the mechanisms that control cell cycle entry and how they might be linked to cell size. The key molecular event that drives cell cycle entry is activation of Cdk1 by G1 cyclins (Richardson et al., 1989; Cross, 1990). There are three G1 cyclins that bind and activate Cdk1 in budding yeast, called Cln1, Cln2, and Cln3 (Hadwiger et al., 1989; Richardson et al., 1989). Transcription of *CLN3* is initiated in early G1, and the Cln3–Cdk1 complex helps trigger transcription of the late G1 cyclins *CLN1* and *CLN2* (Dirick and Nasmyth, 1991). Cln1/2 drive growth of a new daughter cell, which marks commitment to a new round of cell division (Richardson et al., 1989; Cross, 1990; McCusker et al., 2007).

N. Dephoure and T. MacDonough contributed equally to this paper.

Correspondence to Douglas R. Kellogg: dkellogg@ucsc.edu

Abbreviations used in this paper: ACN, acetonitrile; ChIP, chromatin immunoprecipitation; FA, formic acid; FDR, false discovery rate; LC, liquid chromatography; MS, mass spectrometry; m/z, mass per charge; qRT-PCR, quantitative RT-PC; SCX, strong cation exchange.

The Rockefeller University Press $30.00
J. Cell Biol. Vol. 204 No. 3 359–376
www.jcb.org/cgi/doi/10.1083/jcb.201309119

Early evidence pointed to Cln3 as playing a critical role in cell size control. Loss of *CLN3* causes a prolonged delay in entry into the cell cycle. Cell growth continues during the delay, leading to increased cell size (Cross, 1988). Conversely, overexpression of *CLN3* causes premature entry into the cell cycle at a reduced cell size (Cross, 1988; Nash et al., 1988). Together, these observations suggested that Cln3, like Wee1, is a critical dose-dependent regulator of cell size (Cross, 1988; Nash et al., 1988). In this view, cell size in G1 phase could be controlled by mechanisms that link production of active Cln3/Cdk1 to attainment of a critical cell size. Several observations, however, indicate that this kind of model is too simplistic. First, *cln3Δ* cells still show size-dependent entry into the cell cycle (Di Talia et al., 2009; Ferrezuelo et al., 2012). Thus, although *cln3Δ* cells are significantly larger than wild-type cells, small unbudded *cln3Δ* cells spend more time undergoing growth in G1 than larger unbudded cells. In addition, *cln3Δ* cells undergo normal nutrient modulation of cell size, in which cells reduce their size in response to poor nutrients (Jorgensen et al., 2004). Together, these observations indicate that modulation of Cln3 alone is insufficient to explain cell size control in G1.

Although Wee1 and G1 cyclins clearly play roles in cell size control, it is unlikely that they are involved in the mechanisms that determine size. Both are capable of accelerating or delaying the cell cycle in a dose-dependent manner, which suggests that they respond to checkpoint signals that determine the duration of growth at specific phases of the cell cycle. Thus, they appear to be downstream effectors of a global mechanism of cell size control. The nature of this global mechanism has remained deeply mysterious.

We recently discovered that a specific form of PP2A (protein phosphatase 2A) is required for cell size control (Artiles et al., 2009). Canonical PP2A is a trimeric complex composed of a catalytic subunit, a scaffolding subunit, and a regulatory subunit (Zhao et al., 1997; Janssens and Goris, 2001). In budding yeast, there are two regulatory subunits, referred to as Rts1 and Cdc55, that form two distinct complexes: $PP2A^{Rts1}$ and $PP2A^{Cdc55}$ (Zhao et al., 1997). We previously discovered that *rts1Δ* causes increased cell size and a failure to undergo nutrient modulation of cell size (Artiles et al., 2009). In addition, *rts1Δ* causes a prolonged delay in transcription of the G1 cyclin Cln2, a prolonged delay in mitosis, and defects in regulatory phosphorylation of Wee1 (Artiles et al., 2009; Harvey et al., 2011). Together, these observations suggest that $PP2A^{Rts1}$ functions in both G1 and mitotic cell size checkpoints. However, the targets of $PP2A^{Rts1}$ that mediate these functions were unknown. Here, we used proteome-wide mass spectrometry (MS) to identify targets of $PP2A^{Rts1}$. This revealed that $PP2A^{Rts1}$ controls key elements of both cell size checkpoints, which suggests that it functions in the mysterious cell size control mechanisms that send signals to G1 cyclins and Wee1. We further discovered that $PP2A^{Rts1}$ controls the transcription factor Ace2, which likely contributes to mechanisms that link *CLN3* transcription to cell growth.

Results

A proteomic screen for targets of $PP2A^{Rts1}$

To identify targets of $PP2A^{Rts1}$, we used quantitative phosphoproteomics to search for proteins that become hyperphosphorylated in *rts1Δ* cells. Because we previously found that $PP2A^{Rts1}$ is required for control of G1 cyclin transcription, we were particularly interested in G1 targets of $PP2A^{Rts1}$ (Artiles et al., 2009). We therefore synchronized wild-type and *rts1Δ* cells and collected samples for MS 10 min before the G1 cyclin Cln2 appeared, which is when the decision to initiate G1 cyclin transcription is made. Proteolytic peptides from each strain were covalently modified by reductive dimethylation to generate light (wild type) and heavy (*rts1Δ*) stable isotope-labeled pools. After combining, phosphopeptides were enriched by strong cation exchange (SCX) followed by TiO_2 affinity chromatography and identified via liquid chromatography (LC)–MS/MS (Fig. 1 A; Villén and Gygi, 2008; Kettenbach and Gerber, 2011).

The heavy to light ratios of phosphorylated peptides in *rts1Δ* cells versus wild-type cells were $\log_2$ transformed. Thus, positive values indicate increased phosphorylation in *rts1Δ*, whereas negative values indicate decreased phosphorylation. A parallel analysis of sample-matched unphosphorylated peptides was used to generate protein abundance ratios that were used to correct for differences in protein abundance between the two samples (Table S1). Three biological replicates of the experiment were performed, which allowed calculation of average $\log_2$ ratios and SDs for most peptides. The complete dataset appears in Tables S1–S3. Table S1 lists all protein quantification data, Table S2 lists all identified phosphorylation sites along with quantitative data, and Table S3 provides detailed information for each of the 78,204 phosphopeptides that were detected.

A total of 10,807 sites were identified on 2,066 proteins. Of these, 9,255 sites on 1,937 proteins could be quantified. We focused on sites that were quantified in at least two of three biological replicates. This high-quality set includes 5,159 sites on 1,544 proteins (Fig. 1 B). Note that the analysis is not comprehensive; many peptides are not detected as a result of poor ionization, loss during chromatography, or low abundance.

Relative peptide abundances were calculated as the ratio of corresponding heavy and light peptide pairs as determined from their extracted ion chromatograms. A visual representation of this is shown for a single phosphopeptide in Fig. S1. For each phosphorylation site, we calculated an average ratio from all quantified peptides harboring each site. We used a twofold SD from the mean, representing a ∼2.5-fold change in either direction, to define significant changes in phosphorylation (Fig. 1 C). At this threshold, we identified 241 sites on 156 proteins that were hyperphosphorylated in *rts1Δ* cells (Table S4). We observed fewer sites whose phosphorylation decreased: 59 sites on 45 proteins (Table S5).

$PP2A^{Rts1}$ is required for normal regulation of key effectors of cell size control

Table S4 lists proteins that underwent significant hyperphosphorylation in *rts1Δ* cells. It is likely that additional regulated sites whose ratios fell below our cutoff exist in the data. Several of the regulated proteins are linked to known roles of $PP2A^{Rts1}$. For example, $PP2A^{Rts1}$ controls Kin4 in the spindle orientation checkpoint (Chan and Amon, 2009). A site in Kin4, serine 351, was up-regulated nearly threefold in *rts1Δ* cells. $PP2A^{Rts1}$ also controls chromosome cohesion (Yu and Koshland, 2007). Here,

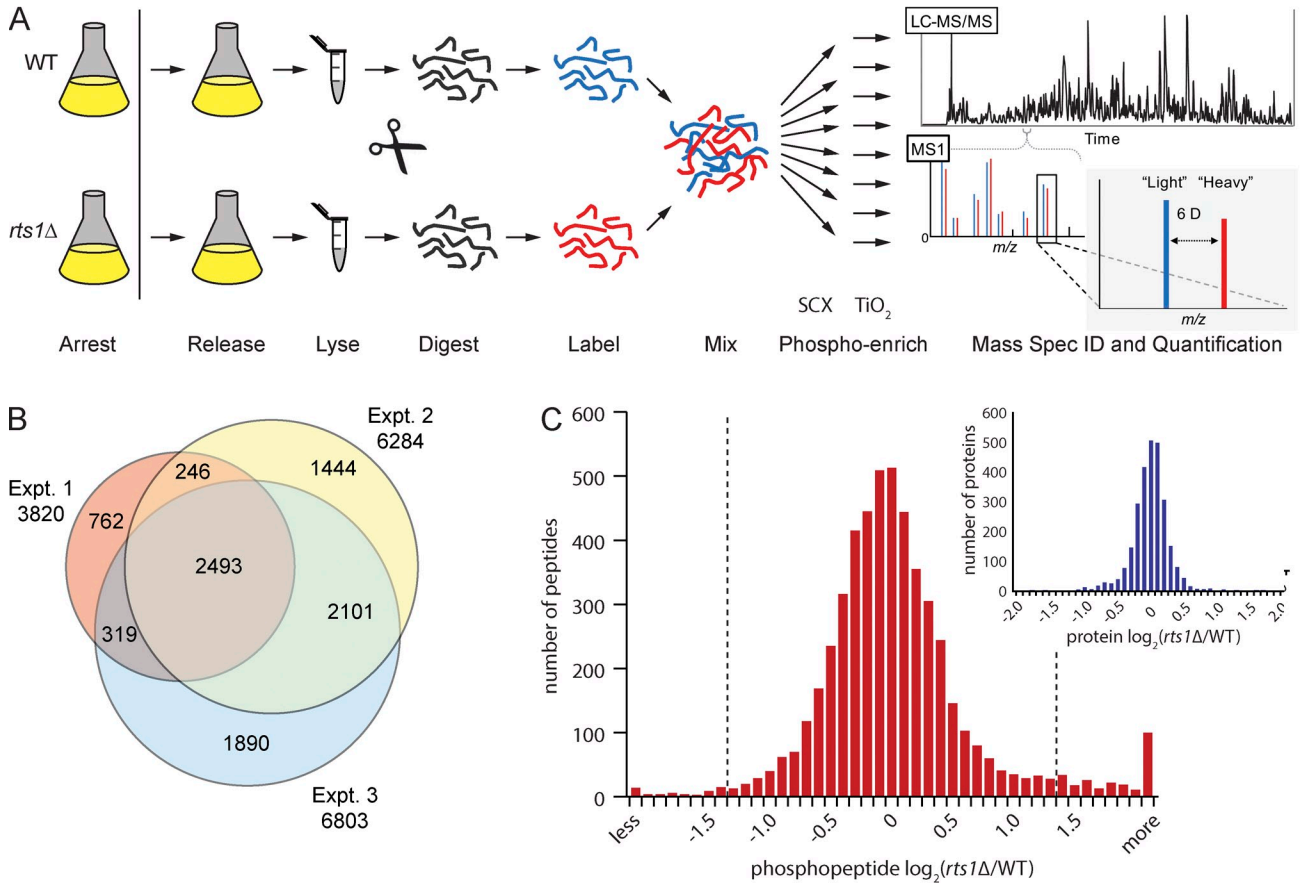

Figure 1. **A phosphoproteomic screen for proteins regulated by PP2A^{Rts1}.** (A) A schematic summary of the approach used to search for targets of PP2A^{Rts1}. (B) A total of 9,255 sites were quantified in three biological replicates. The overlap of sites quantified from each replicate is shown. (C) The $\log_2$ distribution of 5,159 sites quantified in at least two replicates. The area outside the dotted lines indicates sites that change by two SDs or greater. The $\log_2$ distribution of the 2,702 quantified proteins is shown in the inset. Expt., experiment; WT, wild type.

we identified two proteins involved in chromosome cohesion as new targets of PP2A^{Rts1}-dependent regulation: Pds1 and Ulp2.

We focused on targets of PP2A^{Rts1} that could provide clues to its role in cell size control. The analysis identified multiple proteins involved in cell size control in G1, including three factors that control G1 cyclin transcription: Swi4, Swi5, and Ace2. Swi4 is a transcriptional activator of the late G1 cyclins *CLN1* and *CLN2* (Nasmyth and Dirick, 1991; Ogas et al., 1991). Swi5 and Ace2 are related factors that control transcription of genes expressed in late mitosis and early G1 (Dohrmann et al., 1992; Doolin et al., 2001). Ace2 is a repressor of *CLN3* transcription, whereas Swi5 controls transcription of the G1 cyclin Pcl2, which activates Pho85 and acts redundantly with Cln1/2 to promote bud emergence (Aerne et al., 1998; Laabs et al., 2003; Moffat and Andrews, 2004; Di Talia et al., 2009). Bck2, an upstream regulator of *CLN1/2* transcription, was hyperphosphorylated in one of the biological replicates (Table S2; Di Como et al., 1995; Bastajian et al., 2013). Thus, PP2A^{Rts1} appears to control transcription of all of the key G1 cyclins. The analysis also identified Ydj1, which is thought to control Cln3 localization and stability (Yaglom et al., 1996; Vergés et al., 2007). Loss of Ace2, Swi4, or Ydj1 causes defects in cell size control (Breeden and Mikesell, 1991; Caplan and Douglas, 1991; Dohrmann et al., 1992; Di Talia et al., 2009; Ferrezuelo et al., 2012).

The analysis also identified proteins involved in cell size control during mitosis. For example, the inhibitory site on Cdk1 that is phosphorylated by Wee1 showed one of the most dramatic increases, being up-regulated >25-fold in *rts1Δ* cells. Moreover, Swe1, the budding yeast homologue of Wee1, was hyperphosphorylated on multiple sites that were previously found to be required for its activation (Harvey et al., 2005, 2011). This is consistent with our previous finding that *rts1Δ* causes Swe1 to accumulate in a hyperphosphorylated active form, which is the likely cause of a prolonged mitotic delay (Harvey et al., 2011). We also identified three related kinases that are required for Swe1 inactivation: Hsl1, Gin4, and Kcc4 (Ma et al., 1996; Barral et al., 1999; McMillan et al., 1999; Longtine et al., 2000). Loss of these kinases can cause delayed entry into mitosis and severe cell size defects (Altman and Kellogg, 1997; Barral et al., 1999). Loss of these kinases also causes Swe1 to accumulate in a hyperphosphorylated active form, similar to *rts1Δ* (Shulewitz et al., 1999; Okuzaki et al., 2003). Together, these observations suggest that PP2A^{Rts1} controls Swe1 via Hsl1, Gin4, and Kcc4. The fission yeast homologues of Hsl1, Gin4, and Kcc4 are required for nutrient modulation of cell size (Young and Fantes, 1987; Belenguer et al., 1997).

The MS data show that PP2A^{Rts1} controls both of the known targets of cell size control: G1 cyclin expression and

Table 1. **Ace2 phosphorylation sites**

Site	Local sequence	No. identified peptides	No. quantified peptides	No. replicates quantified	Average ratio	SD
S122	SHKRGL**S**GTAIFG	2	2	2	2.51	0.72
T135	FLGHNK**T**LSISSL	1	1	1	2.41	ND
S137	GHNKTL**S**ISSLQQ	2	0	0	ND	ND
S140	KTLSIS**S**LQQSIL	3	0	0	ND	ND
T245	KLVSGA**T**NSNSKP	6	2	1	2.44	ND
S249	GATNSN**S**KPGSPV	6	5	2	0.93	0.02
S253	SNSKPG**S**PVILKT	8	7	2	1.43	0.73
S709	KKSLLD**S**PHDTSP	9	9	3	1.54	0.29
T713	LDSPHD**T**SPVKET	9	7	2	1.62	0.24
S714	DSPHDT**S**PVKETI	4	4	2	1.27	0.05

The table shows all identified and quantified phosphosites in Ace2. The phosphorylated residue is shown in bold in the context of its flanking sequence. Six sites were identified in two out of three biological replicates, and out of those six, four showed increased phosphorylation above the $\log_2$ threshold: S122, S253, S709, and T713.

inhibitory phosphorylation of Cdk1. Thus, $PP2A^{Rts1}$ may be a component of global cell size control mechanisms. Here, we focused on the Ace2 transcription factor. Table 1 shows data for all identified Ace2 phosphorylation sites, which includes four significantly regulated sites: S122, S253, S709, and T713. Ace2 is asymmetrically segregated into the nuclei of small daughter cells, where it is thought to delay cell cycle entry via inhibition of *CLN3* transcription (Laabs et al., 2003; Di Talia et al., 2009). However, regulation of Ace2 has not been linked to signals that relay information about cell growth or size. Ace2 also functions as a transcriptional activator for genes involved in septation (Dohrmann et al., 1992).

Loss of $PP2A^{Rts1}$ causes defects in phosphorylation of the Ace2 transcription factor

To extend the MS data, we assayed Ace2 phosphorylation in synchronized wild-type and *rts1Δ* cells. Phosphorylation of Ace2 causes an electrophoretic mobility shift that can be assayed by Western blotting (Sbia et al., 2008; Mazanka and Weiss, 2010). We first assayed Ace2 after release from a G1 arrest imposed by mating pheromone. The mitotic cyclin Clb2 was assayed in the same samples as a marker for cell cycle progression. In wild-type cells, Ace2 was present at low levels early in the cell cycle and began to accumulate and undergo extensive hyperphosphorylation as cells entered mitosis, consistent with previous studies that Ace2 is phosphorylated by mitotic Cdk1 (Fig. 2 A; O'Conalláin et al., 1999; Sbia et al., 2008; Mazanka and Weiss, 2010). In *rts1Δ* cells, the mitotic hyperphosphorylation of Ace2 was delayed by ∼20 min, consistent with a previously reported G1 delay in *rts1Δ* cells (Artiles et al., 2009). To compare differences in Ace2 phosphorylation during G1, we loaded the initial time points from Fig. 2 A in an intercalated manner (Fig. 2 B). This revealed that a fraction of Ace2 was hyperphosphorylated in *rts1Δ* cells during G1.

We also assayed Ace2 phosphorylation and Clb2 levels after release from a metaphase arrest. Ace2 was phosphorylated in metaphase-arrested wild-type cells and was dephosphorylated as cells exited mitosis (Fig. 2 C). Ace2 underwent a transient phosphorylation at 30 min and became phosphorylated again at 50 min as cells entered the next mitosis. Ace2 was dramatically hyperphosphorylated in *rts1Δ* cells relative to wild-type cells (Fig. 2 C). In addition, Ace2 dephosphorylation and destruction of Clb2 were delayed by ∼20 min in *rts1Δ* cells, which indicated that $PP2A^{Rts1}$ is required for normal mitotic

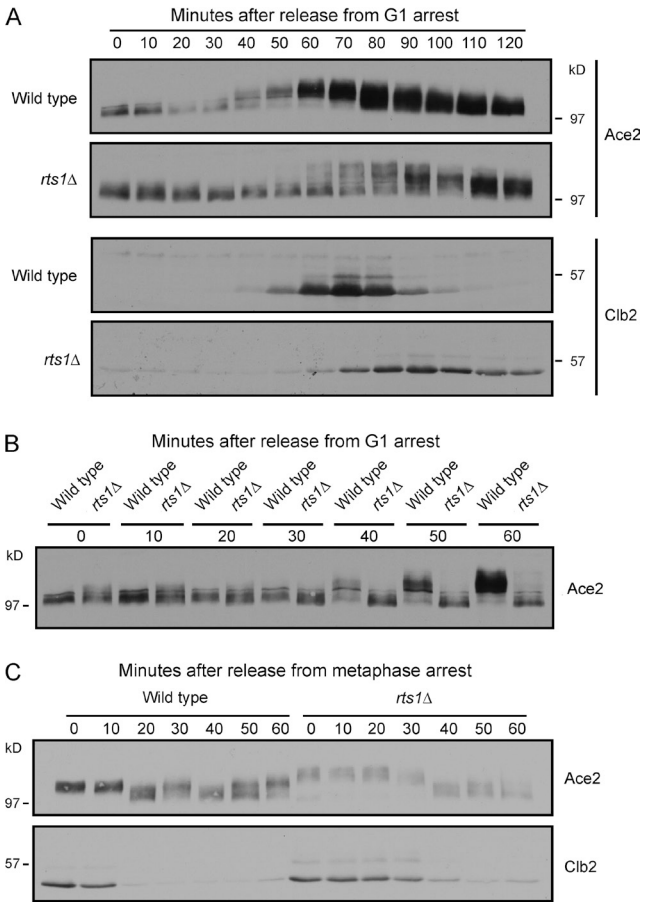

Figure 2. **The Ace2 transcription factor is hyperphosphorylated in *rts1Δ* cells.** (A) Cells were released from a G1 arrest, and the behavior of Ace2 and Clb2 was assayed by Western blotting. (B) The same samples shown in Fig. 2 B were loaded in an intercalated manner to visualize differences between wild-type and *rts1Δ* cells. (C) Cells were released from a metaphase arrest, and the behavior of Ace2 and Clb2 was assayed by Western blotting.

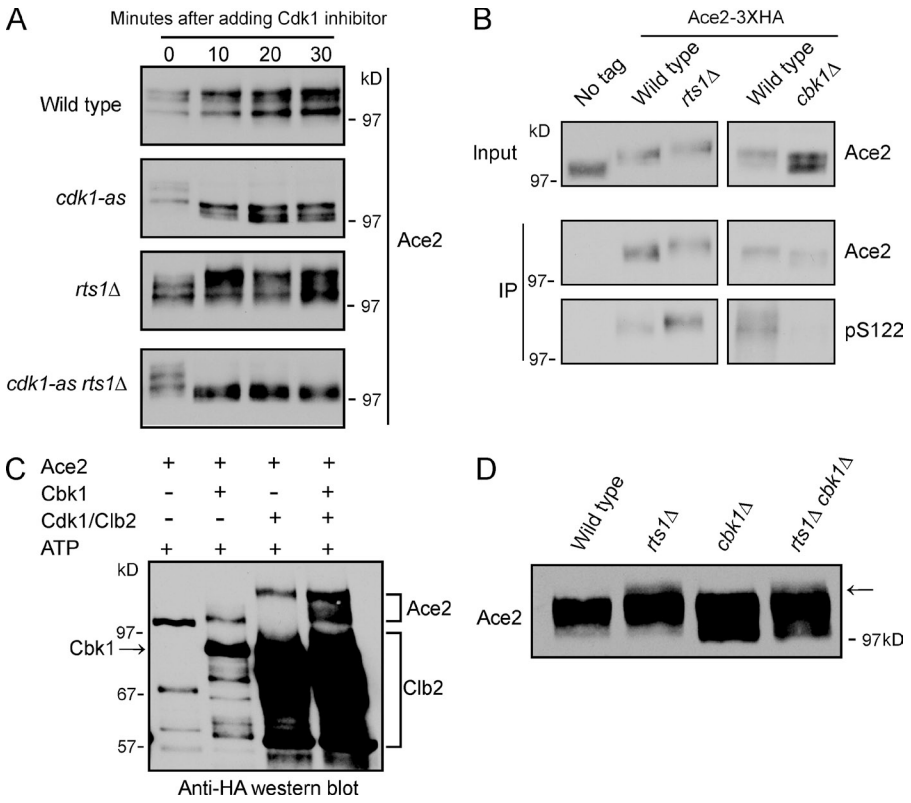

Figure 3. **Multiple kinases contribute to hyperphosphorylation of Ace2 in *rts1Δ* cells.** (A) Samples were taken at the indicated times after addition of 1NM-PP1 to log phase cells, and phosphorylation of Ace2 was assayed by Western blotting. (B) Ace2-3×HA was immunoprecipitated from wild-type, *rts1Δ*, or *cbk1Δ* cells and probed with anti-Ace2 antibody or with an antibody that recognizes phosphorylated S122. Ace2-3×HA was immunoprecipitated from the *cbk1Δ* cells as a control to demonstrate that the phosphospecific antibody recognizes a site phosphorylated by Cbk1. (C) Kinase reactions containing affinity purified Ace2-3×HA, Cbk1-3×HA, and Cdk1/Clb2-3×HA in the indicated combinations were initiated by addition of ATP. Ace2-3×HA phosphorylation was assayed by Western blotting with the anti-HA mouse monoclonal antibody. (D) Cells were grown to log phase at room temperature, and Ace2 phosphorylation was assayed by Western blotting. The arrow indicates a hyperphosphorylated form of Ace2.

exit. Because we did not observe a drop in Ace2 levels as cells traversed G1 after release from a metaphase arrest (Fig. 2 C), it is likely that low levels of Ace2 after release from a G1 arrest (Fig. 2 A) is caused by the prolonged arrest, rather than by a mechanism that degrades Ace2 during G1 in every cell cycle.

Cbk1 contributes to hyperphosphorylation of Ace2 in *rts1Δ* cells

We next searched for the kinase that hyperphosphorylates Ace2 in *rts1Δ* cells. Cdk1 is thought to phosphorylate Ace2 during mitosis to block its nuclear import (O'Conalláin et al., 1999; Sbia et al., 2008; Mazanka and Weiss, 2010). If Cdk1 and $PP2A^{Rts1}$ acted on the same sites, one would predict that dephosphorylation of Ace2 would fail to occur or would occur more slowly when Cdk1 was inactivated in *rts1Δ* cells. To test this, we used an analogue-sensitive allele of *CDK1* (*cdk1-as1*) that can be rapidly and specifically inhibited by addition of 1NM-PP1 (Bishop et al., 2000). Ace2 phosphorylation was assayed after addition of 1NM-PP1 to rapidly growing wild type, *cdk1-as1*, *rts1Δ*, and *cdk1-as1 rts1Δ* cells. Inhibition of Cdk1 caused rapid dephosphorylation of Ace2 in both *cdk1-as1* and *cdk1-as1 rts1Δ* cells (Fig. 3 A). This suggests that Cdk1 and $PP2A^{Rts1}$ do not act on the same sites but does not rule out a more complex model in which $PP2A^{Rts1}$ acts redundantly with another phosphatase on Cdk1 target sites. None of the four high confidence hyperphosphorylated sites on Ace2 correspond to the optimal mitotic Cdk1 consensus site (S/TPXXR/K), although three of the four correspond to the minimal Cdk1 consensus site (S/TP).

Ace2 is also phosphorylated by Cbk1, a member of the NDR/LATS (nuclear Dbf2-related/large tumor suppressor) kinase family that plays roles in bud growth and mitotic exit (Mazanka et al., 2008). During late mitosis, Cbk1 is asymmetrically localized to the daughter nucleus, where it phosphorylates Ace2 on several sites that inhibit nuclear export (Colman-Lerner et al., 2001; Weiss et al., 2002; Mazanka et al., 2008). Cbk1 could therefore inhibit nuclear export of Ace2 to delay *CLN3* transcription in newborn daughter cells. One of the high confidence Ace2 sites corresponds to a Cbk1 consensus site (S122) that is phosphorylated in vitro and in vivo in a Cbk1-dependent manner (Mazanka et al., 2008). Western blotting with a phosphospecific antibody (Mazanka and Weiss, 2010) demonstrated that this site is hyperphosphorylated in *rts1Δ* cells (Fig. 3 B). Thus, Cbk1 is likely responsible for hyperphosphorylating at least one site on Ace2 in *rts1Δ* cells. However, most of the sites that were hyperphosphorylated in *rts1Δ* cells do not correspond to Cbk1 consensus sites, which suggests that multiple kinases may be involved.

To further test the roles of Cdk1 and Cbk1, we reconstituted phosphorylation of Ace2 in vitro. Cdk1 caused a shift in the electrophoretic mobility of Ace2 that was similar to the Cdk1-dependent shift observed in vivo (Fig. 3, A and C). Cbk1 also shifted the electrophoretic mobility of Ace2, but the extent of the shift appeared to be less than the shift caused by *rts1Δ* in vivo (Fig. 3 C). We considered the possibility that efficient phosphorylation of Ace2 by Cbk1 requires priming by Cdk1; however, Cdk1 did not appear to enhance Cbk1 phosphorylation of Ace2 in vitro (Fig. 3 C).

Because there was the possibility that the reconstituted reactions lacked key factors necessary for efficient phosphorylation of Ace2 by Cbk1, we also tested the role of Cbk1 in vivo. We attempted to use an analogue-sensitive allele of Cbk1 to test whether hyperphosphorylation of Ace2 after release from a mitotic

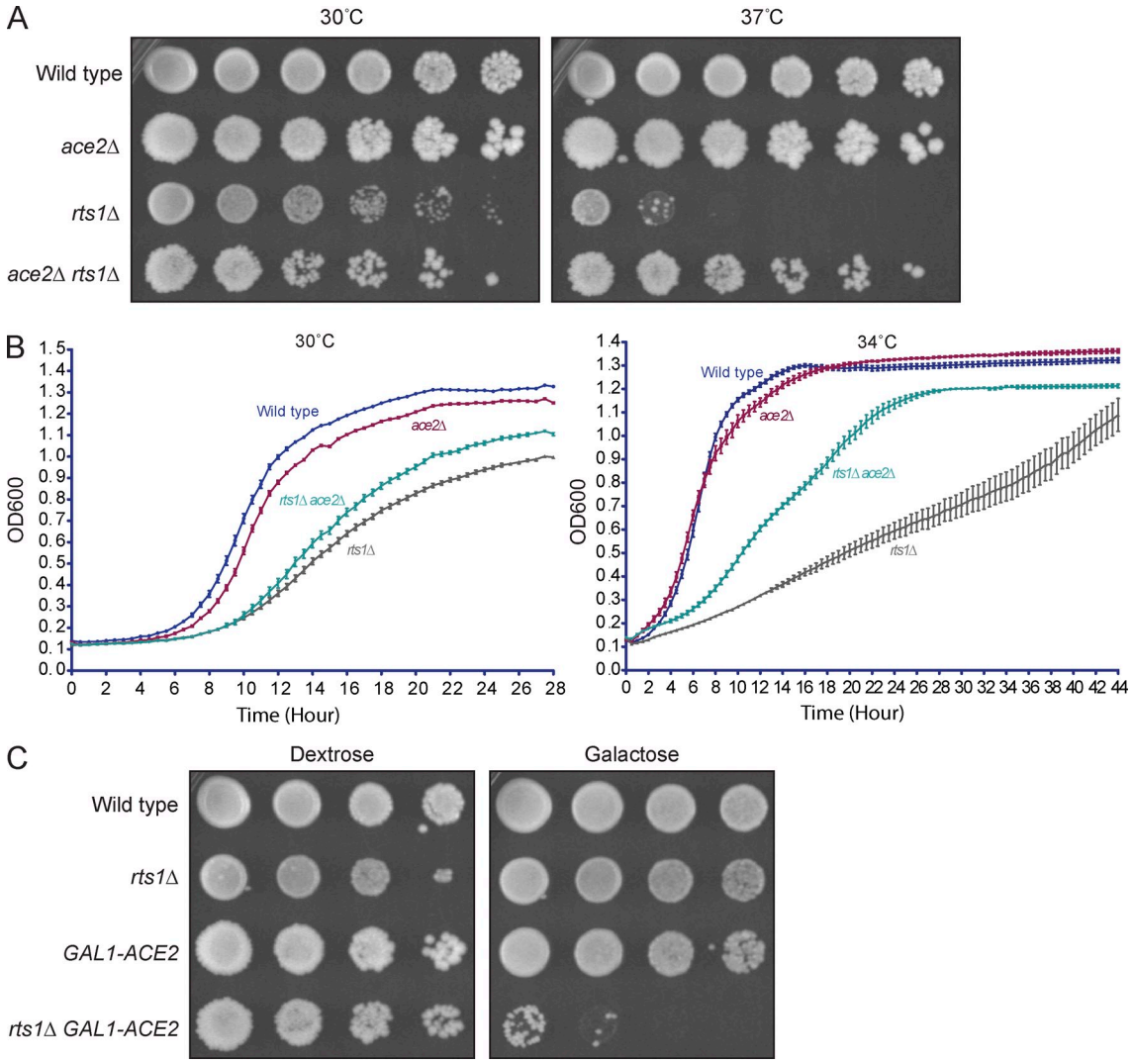

Figure 4. **Genetic analysis suggests that PP2A^{Rts1} is a negative regulator of Ace2.** (A) A series of fivefold dilutions of cells were grown on YPD media at 30 or 37°C. (B) Eight independent colonies grown overnight at 23°C were diluted into fresh medium and grown in a Bioscreen C apparatus. The average growth of the eight cultures was plotted, with SDs shown. (C) A series of fivefold dilutions of cells were grown at 30°C on YEP media containing either dextrose or galactose.

arrest depended on Cbk1 activity. However, for unknown reasons, *rts1Δ cbk1-as* cells expressed very low levels of Ace2 when arrested in mitosis, so we were unable to obtain a clear result. Instead, we assayed hyperphosphorylation of Ace2 in log phase wild-type, *rts1Δ*, *cbk1*Δ, and *rts1Δ cbk1Δ* cells. The majority of Ace2 phosphorylation that can be detected in log phase cells is caused by mitotic Cdk1; however, a hyperphosphorylated form of Ace2 could be faintly detected in both *rts1Δ* and *rts1Δ cbk1Δ* cells (Fig. 3 D, arrow). This observation provides further evidence that Cbk1 cannot be solely responsible for hyperphosphorylation of Ace2 in *rts1Δ* cells.

PP2A^{Rts1} is likely a negative regulator of Ace2

Because *rts1Δ* causes a prolonged G1 delay, we hypothesized that PP2A^{Rts1} inhibits repressor functions of Ace2. In this model, inactivation of PP2A^{Rts1} causes Ace2 to become hyperphosphorylated, which makes it hyperactive as a repressor of *CLN3* transcription. We first used genetics to test this model. If PP2A^{Rts1} is an inhibitor of Ace2, *ace2Δ* could rescue temperature-dependent growth defects caused by *rts1Δ*. To test this, we assayed rate of colony formation in wild-type, *rts1Δ*, *ace2Δ*, and *rts1Δ ace2Δ* cells at 30 and 37°C. We found that *ace2Δ* partially rescued the temperature-dependent growth defect caused by *rts1Δ* (Fig. 4 A). Because *ace2Δ* causes a cell separation defect, colonies could appear larger because they start from a clump of cells rather than a single cell. We therefore used a Bioscreen apparatus to measure rates of growth of each strain. This confirmed that *ace2Δ* partially rescued the slow growth phenotype of *rts1Δ* cells at both 30 and 34°C (Fig. 4 B).

We also discovered that overexpression of Ace2 from the *GAL1* promoter was lethal in *rts1Δ* cells, consistent with the idea that PP2A^{Rts1} inhibits transcriptional repressor functions of Ace2 (Fig. 4 C). The lethality of *ACE2* overexpression in *rts1Δ* suggests that hyperactive Ace2 must have targets in addition to *CLN3* because deletion of *CLN3* alone is not lethal.

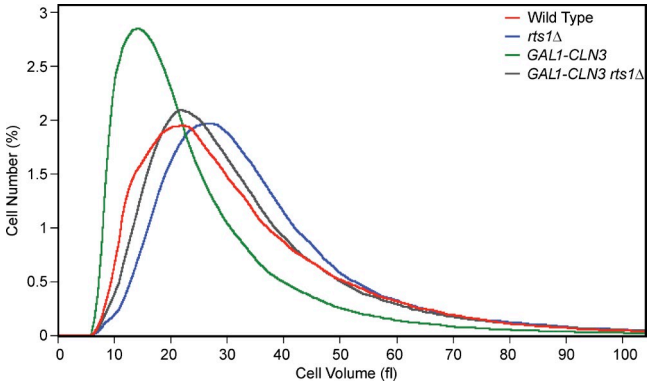

Figure 5. **Overexpression of *CLN3* partially rescues the cell size defects caused by *rts1Δ*.** Cells were grown to log phase in media containing 2% galactose, and cell size distributions were determined using a Coulter counter. Each plot represents the average of three independent biological replicates in which three independent samples were analyzed for each strain.

Overexpression of *CLN3* partially rescues cell size defects caused by *rts1Δ*

Loss of *RTS1* or *CLN3* causes cells to become abnormally large (Cross, 1988; Artiles et al., 2009). We hypothesized that hyperactive Ace2 in *rts1Δ* cells causes failure to produce normal levels of Cln3, leading to increased cell size. To test this, we overexpressed *CLN3* from the *GAL1* promoter in *rts1Δ* cells. This reduced the size of *rts1Δ* cells to nearly the same size as wild-type cells, consistent with the hypothesis (Fig. 5). A previous study found that *CLN3* overexpression causes cells to become significantly smaller than wild-type cells (Fig. 5; Tyers et al., 1992). Thus, *GAL1-CLN3* does not cause the same size reduction in wild-type and *rts1Δ* cells, which indicates that cell size defects caused by *rts1Δ* are not caused solely by a failure to produce normal levels of Cln3. This is consistent with the discovery that $PP2A^{Rts1}$ controls diverse pathways required for cell size control.

$PP2A^{Rts1}$ is required for normal control of Cln3 protein and mRNA levels

To further test the hypothesis that $PP2A^{Rts1}$ controls production of Cln3 via Ace2, we assayed *CLN3* mRNA accumulation in wild-type, *rts1Δ*, *ace2Δ*, and *rts1Δ ace2Δ* cells after release from a G1 arrest. *CLN3* mRNA levels were assayed both by quantitative RT-PCR (qRT-PCR) and by Northern blotting, which gave similar results. Accumulation of Cln3-6×HA protein was assayed in identical time courses, and the mitotic cyclin Clb2 was assayed in the same samples to provide a marker for cell cycle progression.

In wild-type cells, *CLN3* mRNA and protein peaked in G1 at 20–30 min (Figs. 6, A–C; and S2). There was a second peak of *CLN3* mRNA and protein later in the cell cycle that appeared at the same time as peak levels of the mitotic cyclin Clb2, indicating that Cln3 is produced in mitosis (Fig. 6, A–D). In *rts1Δ* cells, accumulation of *CLN3* mRNA and protein was reduced and delayed (Figs. 6, A–C; and S2). The defect in *CLN3* mRNA accumulation caused by *rts1Δ* at 20 min showed a statistically significant rescue by *ace2Δ* (Fig. 6 B). In addition, *ace2Δ*

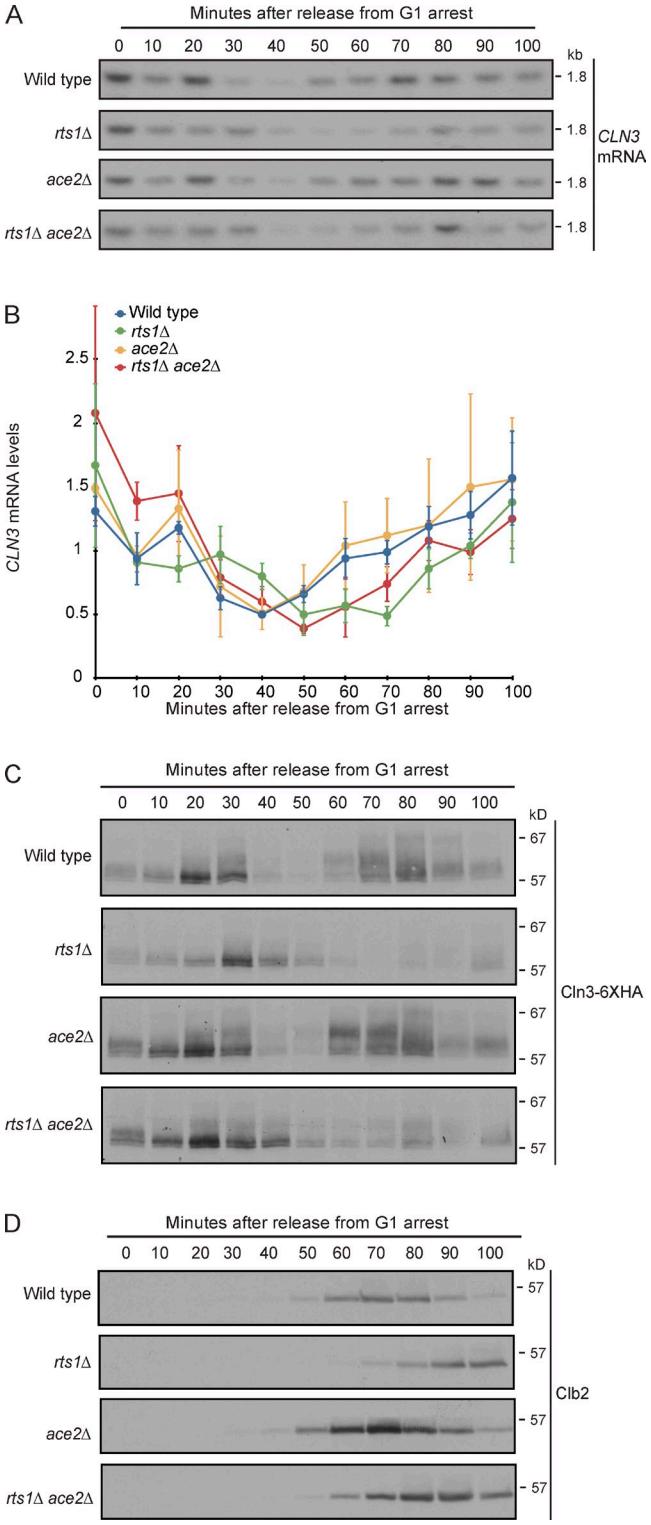

Figure 6. **$PP2A^{Rts1}$ is required for normal control of *CLN3* mRNA and protein levels in cells released from a G1 arrest.** (A–D) Wild-type, *rts1Δ*, *ace2Δ*, and *rts1Δ ace2Δ* cells were released from G1 arrest at 30°C, and the behavior of *CLN3* mRNA was assayed by Northern blotting (A) or qRT-PCR (B). Independent samples were probed for Cln3-6×HA (C) and Clb2 (D) by Western blotting. The Cln3-6×HA and Clb2 Western blots were from the same samples to allow direct comparison of the timing of cell cycle events. Loading controls for the Northern blot and the Western blots are shown in Fig. S2. Error bars in B indicate the SDs of three biological replicates.

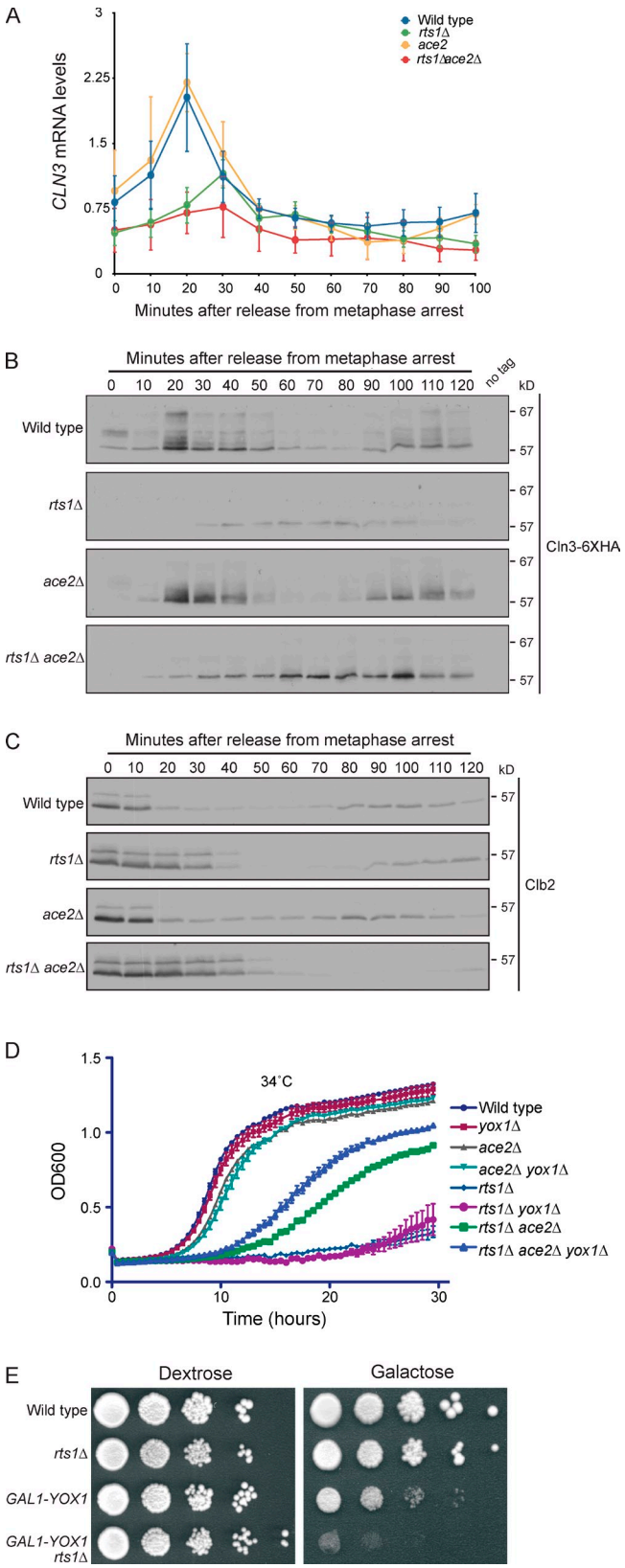

Figure 7. **PP2A^{Rts1} is required for normal control of *CLN3* mRNA and protein levels in cells released from a metaphase arrest.** (A–C) *GAL-CDC20*, *GAL-CDC20 rts1Δ*, *GAL-CDC20 ace2Δ*, and *GAL-CDC20 ace2Δ rts1Δ* cells were released from a metaphase arrest at 30°C, and samples were analyzed by qRT-PCR (A). Independent samples were probed for Cln3-6×HA (B) and Clb2 (C) by Western blotting. The Cln3-6×HA and Clb2 Western blots were from the same samples to allow direct comparison of the timing of cell cycle events. (D) Cell growth rate was analyzed using a Bioscreen C apparatus. (E) A series of 10-fold dilutions of cells were grown at 25°C on YEP media containing either dextrose or galactose. Error bars in A indicate the SDs of three biological replicates. Error bars in D indicate SDs of four independent cultures.

advanced the peak of Cln3 protein early in the cell cycle in *rts1Δ* cells, consistent with a rescue of *CLN3* mRNA levels. However, defects in *CLN3* mRNA accumulation that occurred later in the cell cycle (time points 50–100 min) were not rescued by *ace2Δ* (Fig. 6, A–C).

We performed similar experiments in cells released from a metaphase arrest. In wild-type cells, *CLN3* mRNA and protein were present at the metaphase arrest and then increased as Clb2 levels declined, reaching a peak 20 min after release from the arrest (Fig. 7, A–C). Cln3 protein was present throughout most of G1, decreased before mitosis, and then accumulated again during the second mitosis. The decline in *CLN3* mRNA and protein at 30 min was correlated with hyperphosphorylation of Ace2, consistent with a role for Ace2 hyperphosphorylation in repression of *CLN3* transcription (Figs. 2 C and 7, A and B, compare wild-type samples). In *rts1Δ* cells, destruction of Clb2 was delayed, indicating a delay in exit from mitosis, and *CLN3* mRNA and protein failed to accumulate to normal levels as cells exited mitosis (Fig. 7, A–C). Defects in *CLN3* mRNA accumulation in *rts1Δ* cells were not rescued by *ace2Δ* (Fig. 7, A and B).

Together, these observations show that *ace2*Δ may rescue some, but not all, defects in *CLN3* mRNA accumulation caused by *rts1Δ*. A possible explanation is that PP2A^{Rts1} controls an additional repressor of *CLN3* transcription. The only other known repressor of *CLN3* transcription is Yox1 (Pramila et al., 2002; Bastajian et al., 2013). The MS analysis identified a hyperphosphorylated Yox1 peptide in *rts1Δ* cells with high confidence in one of the biological replicates (Table S3). In addition, *yox1Δ* improved the growth rate of *rts1Δ ace2Δ* cells at 34°C (Fig. 7 D). Finally, *rts1Δ* increased the toxicity caused by expression of *YOX1* from the *GAL1* promoter (Fig. 7 E). PP2A^{Rts1} may therefore control multiple repressors of *CLN3* transcription.

PP2A^{Rts1} is required for normal control of transcriptional activator functions of Ace2

In addition to its repressor functions, Ace2 is a transcriptional activator for genes involved in cell separation, including *CTS1* (Dohrmann et al., 1992). To test whether PP2A^{Rts1} controls transcriptional activator functions of Ace2, we assayed *CTS1* mRNA levels in wild-type, *rts1Δ*, *ace2Δ*, and *rts1Δ ace2Δ* cells after release from a G1 arrest (Fig. 8). Levels of *CTS1* mRNA showed a significant increase in *rts1Δ* cells that was dependent on *ACE2*. Thus, Ace2 is hyperactive as a transcriptional activator in *rts1Δ* cells.

PP2A^{Rts1} is required for normal binding of Ash1 to the *CLN3* promoter

Ace2 is thought to collaborate with Ash1 to repress *CLN3* transcription (Di Talia et al., 2009). Like Ace2, Ash1 is asymmetrically segregated into the daughter cell at the end of cell division

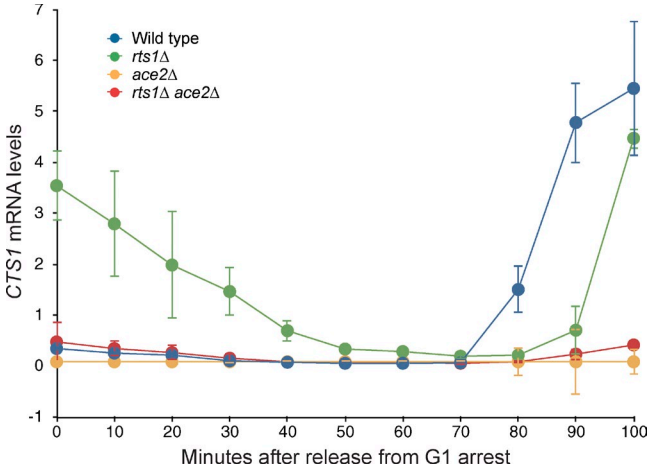

Figure 8. **PP2A^{Rts1} is required for normal control of *CTS1* mRNA levels.** Wild-type, *rts1Δ*, *ace2Δ*, and *rts1Δ ace2Δ* cells were released from a G1 arrest at 30°C, and the behavior of *CTS1* mRNA was assayed by qRT-PCR. Error bars indicate the SDs of three biological replicates.

(Bobola et al., 1996). Chromatin immunoprecipitation (ChIP) experiments have shown that Ace2 and Ash1 bind to the *CLN3* promoter (Di Talia et al., 2009). To further investigate regulation of *CLN3* transcription by PP2A^{Rts1}, we assayed binding of Ace2 and Ash1 to the *CLN3* promoter. Loss of Rts1 did not cause significant effects on binding of Ace2 to the *CLN3* promoter; however, binding of Ash1 was significantly increased (Fig. 9, A and B). In addition, binding of Ace2 was dependent on Ash1, and binding of Ash1 was strongly dependent on Ace2 (Fig. 9, C and D). These findings suggest that hyperphosphorylation of Ace2 causes increased recruitment of Ash1, leading to transcriptional repression.

Ace2 is hyperphosphorylated in small unbudded daughter cells

The preceding experiments show that Ace2 is hyperphosphorylated in *rts1Δ* cells, which likely activates it to repress transcription of *CLN3*. We next investigated regulation of Ace2 in wild-type cells. It is thought that Ace2 causes a G1 delay in small daughter cells by repressing *CLN3* transcription (Laabs et al., 2003; Di Talia et al., 2009). However, the signals that control the duration of the delay are unknown. The discovery that PP2A^{Rts1} controls Ace2 suggested that it could play a role in determining the duration of the G1 delay. We reasoned that one way to test this would be to monitor Ace2 hyperphosphorylation, as well as levels of *CLN3* mRNA and protein, during G1 in newborn daughter cells. If PP2A^{Rts1} plays a role in enforcing a G1 delay, Ace2 should be hyperphosphorylated in newborn daughter cells and dephosphorylation of Ace2 should be correlated with accumulation of Cln3.

Cells synchronized via a cell cycle arrest cannot be used to study events that occur in small newborn daughter cells because cells grow during the arrest. To circumvent this problem, we used centrifugal elutriation to isolate small daughter cells. To enrich for very small daughter cells, the cells were grown in media containing a poor carbon source before elutriation. After isolation, the cells were released into rich media, and samples were taken to assay Ace2 phosphorylation and levels of *CLN3* mRNA and protein as the cells underwent growth and entry into the cell cycle. We also measured cell size as a function of time to monitor cell growth and the fraction of cells undergoing bud emergence to determine when cells enter the cell division cycle. We used Northern blotting to assay *CLN3* mRNA levels because qRT-PCR requires normalization to an internal standard RNA, which could undergo significant changes as cells grow. By using Northern blotting to probe the same fraction of total RNA at each time point, we could assay levels of *CLN3* mRNA per cell.

The small newborn daughter cells underwent continuous growth and initiated bud emergence at 130 min (Fig. 10, A and B). Ace2 was hyperphosphorylated in the small unbudded cells and underwent gradual dephosphorylation (Fig. 10 C). Maximal dephosphorylation of Ace2 occurred at 70–80 min. Cln3 was first detectable at 10 min and then accumulated gradually, reaching peak levels around the time of maximal Ace2 dephosphorylation (Fig. 10 C). Thus, Ace2 dephosphorylation and Cln3 protein accumulation occurred gradually during growth and were correlated. *CLN3* mRNA accumulated gradually during growth, similar to Cln3 protein (Fig. 10 D). We consistently observed a transient increase in *CLN3* mRNA at 5 min, and Cln3 protein began to accumulate shortly thereafter. This burst of *CLN3* mRNA was not correlated with Ace2 phosphorylation.

As expected, the mitotic cyclin Clb2 was not detectable, which indicates that phosphorylation of Ace2 in this context was not caused by mitotic Cdk1 activity. It was not possible to isolate unbudded *rts1Δ* cells because of their severe cell size defects: centrifugal elutriation yielded a mixture of budded and unbudded cells that were of similar size.

Discussion

Identification of PP2A^{Rts1} targets by proteome-wide MS

To identify targets of PP2A^{Rts1}-dependent regulation, we used quantitative proteome-wide MS to search for proteins that undergo changes in phosphorylation in *rts1Δ* cells. Proteome-wide MS should prove to be a powerful tool for identifying phosphatase targets because one searches for proteins that undergo hyperphosphorylation, which is unlikely to be a result of indirect or toxic effects caused by inactivation of the phosphatase.

The analysis identified 156 proteins that undergo significant hyperphosphorylation when PP2A^{Rts1} is inactivated. These likely include direct targets of PP2A^{Rts1} but also appear to delineate entire pathways regulated by PP2A^{Rts1}. For example, several components of a pathway that regulates mitosis via Cdk1 inhibitory phosphorylation were identified. In this pathway, three related kinases called Gin4, Hsl1, and Kcc4 promote entry into mitosis by inactivating Swe1. Gin4 and Hsl1 are controlled by the septins, which were also identified as potential targets of PP2A^{Rts1}-dependent regulation (Table S2). Previous work found that *rts1Δ* causes a mitotic delay and defects in Swe1 phosphorylation; however, the underlying mechanisms were unknown. The MS data suggest that PP2A^{Rts1} regulates mitosis via a pathway that includes the septins, Gin4/Hsl1/Kcc4, and Swe1.

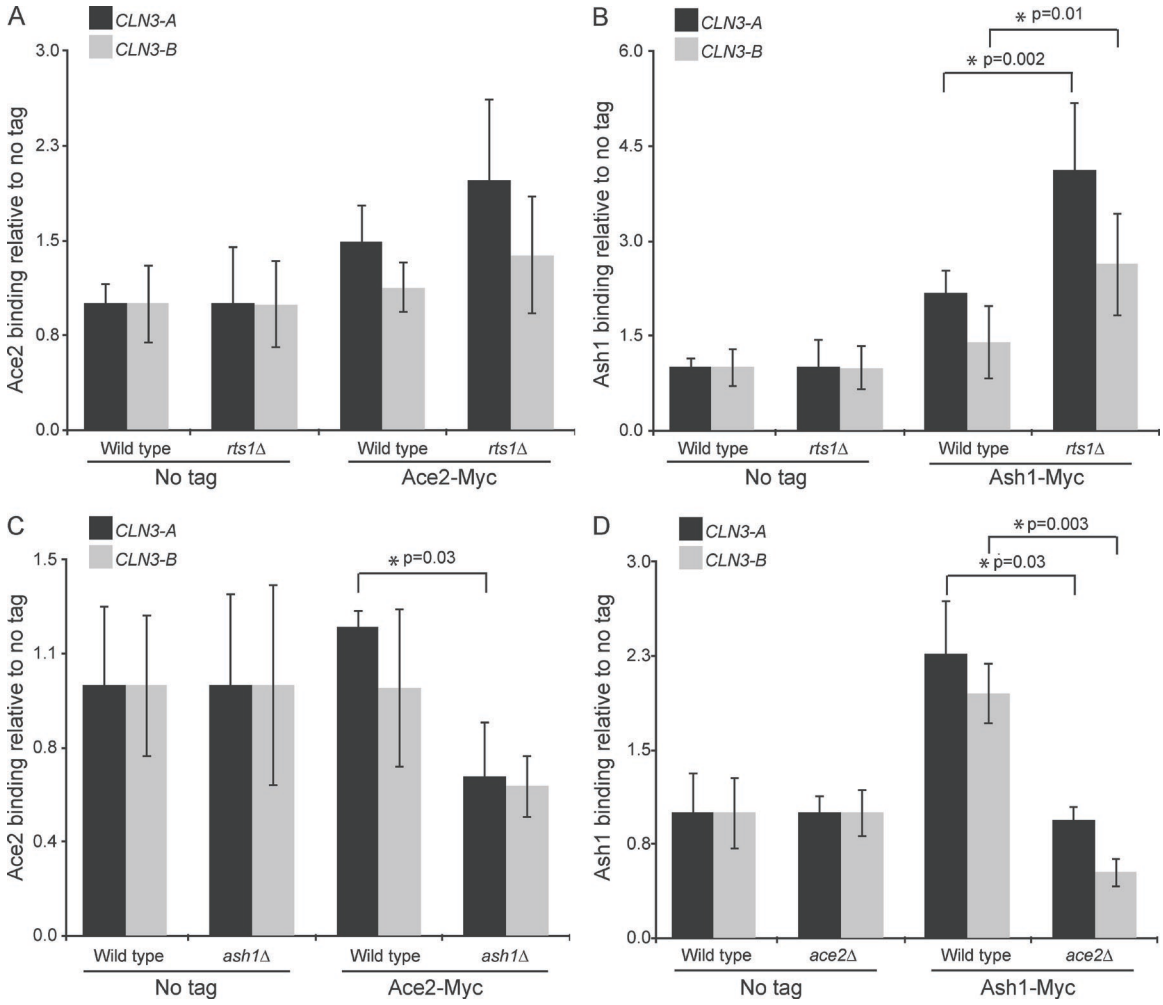

Figure 9. **Loss of PP2A^{Rts1} causes increased binding of Ash1 to the *CLN3* promoter.** ChIP experiments were performed using Ace2-Myc, Ash1-Myc, or untagged control strains. Transcription factor binding was measured for two regions of the *CLN3* promoter, *CLN3*-A (−1,026 to −830) and *CLN3*-B (−853 to −642), in distance from the ATG. Data from at least three replicates were analyzed by an unpaired two-tailed *t* test to test for statistically significant differences. Error bars indicate SDs.

In addition to identifying targets of PP2A^{Rts1}-dependent regulation, the MS identified 10,807 phosphorylation sites on 2,066 proteins. These sites significantly expand phosphorylation site data in budding yeast. Nevertheless, it must be kept in mind that proteome-wide MS is not comprehensive. Thus, little can be inferred from the absence of proteins or sites in the data. In addition, the analysis generally does not provide sufficient sequence coverage to warrant mutagenesis of identified sites to test their functions. Rather, further site mapping must be performed using purified proteins to yield a more comprehensive identification of sites.

PP2A^{Rts1} as a master regulator of cell size control pathways

Swe1 and the G1 cyclins play important roles in mechanisms that control cell size. Both serve as downstream effectors of cell size control mechanisms that accelerate or delay the cell cycle to allow more or less time for cell growth. The cell size control mechanisms that signal to Swe1 and the G1 cyclins have proven remarkably difficult to discover.

In previous work, we found that PP2A^{Rts1} is required for normal control of cell size as well as nutrient modulation of cell size (Artiles et al., 2009). Here, we discovered that PP2A^{Rts1} regulates pathways that control both Swe1 and G1 cyclins. Together, these observations suggest the possibility that PP2A^{Rts1} is a component of the enigmatic cell size control mechanisms that signal to Swe1 and G1 cyclins.

In G1 phase, PP2A^{Rts1} controls phosphorylation of two key transcription factors for G1 cyclins: Ace2 and Swi4. Ace2 is a repressor of *CLN3* transcription (Laabs et al., 2003; Di Talia et al., 2009), whereas Swi4 is a transcriptional activator for late G1 cyclins *CLN1* and *CLN2* (Nasmyth and Dirick, 1991; Ogas et al., 1991). Because Cln3 appears first and helps promote transcription of *CLN1* and *CLN2*, it was initially thought that size control in G1 works through *CLN3*. However, although *cln3Δ* cells are abnormally large, they still show size-dependent entry into the cell cycle and nutrient modulation of cell size, which

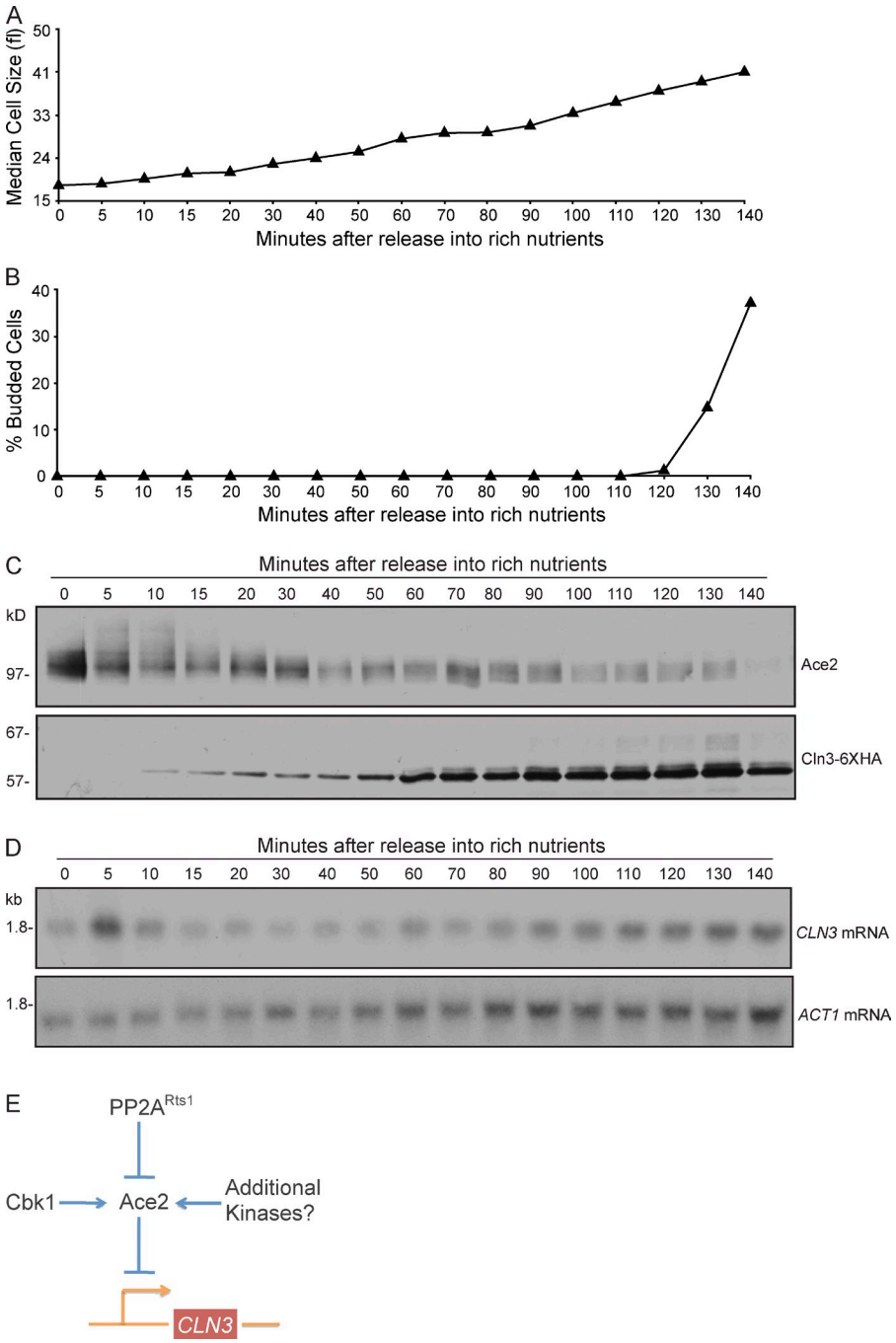

Figure 10. **Ace2 is hyperphosphorylated in small unbudded daughter cells.** Small unbudded cells in G1 were isolated by centrifugal elutriation and released into YPD medium at 25°C. (A) Cell size was analyzed using a Coulter counter and plotted as a function of time. (B) The percentage of budded cells was plotted as a function of time. (C) Ace2 phosphorylation and Cln3-6×HA levels were assayed by Western blotting. All samples in A–C were taken from the same time course. (D) Samples from an independent time course were probed for *CLN3* mRNA. The same membrane was probed for *ACT1* mRNA as a loading control. (E) A model for PP2A^{Rts1}-dependent mechanisms that control *CLN3* transcription via Ace2. For simplicity, mitotic regulation of Ace2 by Cdk1 is not shown in the model.

shows that cell size control in G1 cannot work solely through *CLN3* (Nasmyth and Dirick, 1991; Jorgensen et al., 2004; Di Talia et al., 2009; Ferrezuelo et al., 2012). The discovery that PP2A^{Rts1} controls both Ace2 and Swi4 suggests that a common mechanism could link transcription of both early and late G1 cyclins to cell size or growth. Thus, size dependent entry into the cell cycle in *cln3Δ* cells could work through PP2A^{Rts1}- and Swi4-dependent control of *CLN1* and *CLN2* transcription.

In mitosis, PP2A^{Rts1} regulates a pathway that controls inhibitory phosphorylation of Cdk1. Although much emphasis has been placed on control of cell size at G1 in budding yeast, it is likely that size is also controlled in mitosis. Loss of Swe1 or regulators of Swe1 causes defects in cell size (Ma et al., 1996; Shulewitz et al., 1999; Sreenivasan and Kellogg, 1999; Longtine et al., 2000; Jorgensen et al., 2002; Harvey and Kellogg, 2003; Kellogg, 2003; Harvey et al., 2005). Moreover, nutrients almost certainly modulate cell size at both G1 and mitosis. Classic experiments performed over 30 years ago discovered that daughter cells exit mitosis at a smaller size in poor nutrients (Johnston et al., 1977). More recent work has confirmed that the smallest cells in a population of cells growing in poor nutrients are smaller than the smallest cells in rich nutrients, which can only occur if daughter cells exit mitosis at a smaller size (see, for example, Fig. 3 A in Jorgensen et al. [2004] or Fig. 11 A in Artiles

et al. [2009]). This suggests the existence of a mechanism that drives progression through mitosis at a smaller bud size when cells are growing in poor nutrients. Because $PP2A^{Rts1}$ is required for nutrient modulation of cell size and regulates mitosis, it may be an essential component of this mechanism. $PP2A^{Rts1}$ appears to control mitosis via the related kinases Gin4, Hsl1, and Kcc4. Fission yeast homologues of these kinases (Cdr1 and Cdr2) are required for nutrient modulation of cell size at entry into mitosis, which suggests a conserved mechanism (Young and Fantes, 1987).

$PP2A^{Rts1}$ controls G1 cyclin transcription via the Ace2 transcription factor

We focused on Ace2 as a starting point for characterizing proteins controlled by $PP2A^{Rts1}$. Ace2 is thought to delay cell cycle entry in small daughter cells via repression of *CLN3* transcription (Colman-Lerner et al., 2001; Laabs et al., 2003). The signals that control the length of the Ace2-dependent delay could control cell size but have been largely unknown. Our analysis suggests that $PP2A^{Rts1}$ controls Ace2 and likely influences the duration of G1 and cell size.

Diverse experiments support a model in which hyperphosphorylated Ace2 is active as a repressor of *CLN3* transcription and that $PP2A^{Rts1}$ dephosphorylates Ace2 to promote *CLN3* transcription (Fig. 10 E). In *rts1Δ* cells, Ace2 was hyperphosphorylated, which correlated with decreased *CLN3* mRNA and protein. In wild-type cells, there was a decrease in *CLN3* mRNA and protein 30 min after release from metaphase arrest that correlated with Ace2 hyperphosphorylation. Finally, in small unbudded cells undergoing growth, dephosphorylation of Ace2 occurred gradually and was correlated with gradually increasing Cln3 protein levels.

Genetic analysis provided additional support for the model: overexpression of *ACE2* was lethal in *rts1Δ* cells, and *ace2Δ* partially rescued the reduced growth rate of *rts1Δ* cells at elevated temperatures. In addition, *ace2Δ* rescued defects in *CLN3* mRNA levels in *rts1Δ* cells early in the cell cycle. However, *ace2Δ* did not cause increased *CLN3* mRNA levels in wild-type cells, and it did not rescue reduced levels of *CLN3* mRNA in *rts1Δ* cells exiting mitosis. There are several potential explanations for these observations. First, previous work suggests that Ace2 represses *CLN3* transcription only in small unbudded daughter cells; however, we were not able to test effects of *rts1Δ* and *ace2Δ* upon *CLN3* transcription in small daughter cells for two reasons. First, small daughter cells grow during cell cycle arrests and are therefore lost in synchronized cells. Second, *ace2Δ* and *rts1Δ* cause cell clumping or size defects that preclude isolation of small daughter cells by centrifugal elutriation. Thus, we could not analyze the effects of *rts1Δ* and *ace2Δ* in the context most likely to show strong effects. Another consideration is that $PP2A^{Rts1}$ could also activate factors that promote *CLN3* transcription, in which case inactivation of the repressor would not be sufficient to rescue *CLN3* mRNA levels in *rts1Δ* cells. Finally, $PP2A^{Rts1}$ could regulate multiple repressors of *CLN3* transcription. Consistent with this, we found evidence that $PP2A^{Rts1}$ controls Yox1, another repressor of *CLN3* transcription (Pramila et al., 2002; Bastajian et al., 2013). The *CLN3* gene has an unusually large 5′ untranslated region and is subject to complex regulation (Polymenis and Schmidt, 1997).

What is the kinase that hyperphosphorylates Ace2 in *rts1Δ* cells? Previous work found that Ace2 is phosphorylated by Cbk1, which drives asymmetric localization of Ace2 into daughter cell nuclei (Mazanka et al., 2008). There is also evidence that Cbk1 controls additional Ace2 functions (Mazanka et al., 2008). The MS identified a Cbk1 target site (S122), and Western blotting with a phosphospecific antibody confirmed that the site is hyperphosphorylated in *rts1Δ* cells. However, purified Cbk1 did not appear to be capable of phosphorylating Ace2 in vitro to the same extent observed in vivo in *rts1Δ* cells. In addition, the MS identified numerous sites that have not been attributed to Cbk1. Thus, it is likely that at least one additional kinase regulates Ace2. We found no clear evidence that hyperphosphorylation of Ace2 in *rts1Δ* cells is caused by Cdk1. Moreover, the *rts1Δ* phenotype is not consistent with hyperphosphorylation of Ace2 on mitotic Cdk1 sites because previous work suggests that this should lead to constitutive cytoplasmic localization of Ace2, where it could not repress *CLN3* transcription (O'Conalláin et al., 1999; Sbia et al., 2008).

$PP2A^{Rts1}$ could act directly on Ace2, or it could act further upstream to inhibit a kinase or activate a phosphatase that acts on Ace2. We found that purified $PP2A^{Rts1}$ was not able to dephosphorylate Ace2; however, we could not demonstrate that the $PP2A^{Rts1}$ was active, so the experiment was inconclusive.

$PP2A^{Rts1}$ may contribute to gradual Cln3 accumulation during growth of small cells

Cln3 has been difficult to detect by Western blotting so its behavior during the cell cycle has been little characterized. We used highly sensitive Western blotting techniques to gain an unprecedented view of Cln3 protein during the cell cycle. This revealed that Cln3 shows significant periodic oscillations. One peak of Cln3 occurs in G1, as expected for a G1 cyclin, and a second peak occurs as the mitotic cyclin Clb2 reaches peak levels. The functions of Cln3 during mitosis are unknown.

We also assayed Cln3 and Ace2 during growth of newborn daughter cells. An important hypothesis for cell size control suggests that Cln3 levels are proportional to cell growth or size and that cell cycle entry is triggered when Cln3 levels reach a threshold (Jorgensen and Tyers, 2004; Turner et al., 2012). However, Cln3 has never been assayed in growing newborn daughter cells to test this model. We found that Cln3 was initially absent in newborn daughter cells and then accumulated gradually during growth. Cln3 reached peak levels at ∼90 min, and bud emergence began 40 min later. The striking correlation between Cln3 protein levels and cell growth is consistent with the Cln3 threshold model. The delay between peak Cln3 levels and bud emergence may correspond to a previously described size-independent delay in G1 that occurs before bud emergence (Di Talia et al., 2007, 2009). Alternatively, the delay may reflect additional size-dependent mechanisms that regulate the activity or localization of Cln3 (Vergés et al., 2007). Mechanisms that restrain the ability of *CLN3* to trigger cell cycle entry during early daughter cell growth may play a role in setting a size threshold.

Table 2. **Strains used in this study**

Strain	MAT	Genotype	Reference or source
DK186	a	*bar1*	Altman and Kellogg, 1997
DK351	a	*bar1 cdk1::cdk1-as1*	Bishop et al., 2000
DK647	a	*bar1 rts1Δ::kanMX6*	Artiles et al., 2009
DK751	a	*bar1 CLN2-3×HA::LEU2 rts1Δ::kanMX6*	Artiles et al., 2009
DK968	a	*bar1 cdk1::cdk1-as1 rts1Δ::HIS*	Bishop et al., 2000
DK1307	a	*bar1 CLN2-3×HA::LEU2 rts1Δ::HIS*	Artiles et al., 2009
DK1907	a	*bar1 CLN2-3×HA::LEU2 rts1Δ::HIS ace2Δ::kanMX4*	This study
DK1908	a	*bar1 CLN2-3×HA::LEU2 ace2Δ::kanMX4*	This study
DK1929	a	*bar1 CLN2-3×HA::LEU2 GAL1-ACE2::HIS5*	This study
DK1930	a	*bar1 CLN2-3×HA::LEU2 GAL1-ACE2::HIS5 rts1Δ::kanMX6*	This study
DK2010	a	*bar1* pDK93A [*GAL1-CLN3::URA*]	This study
DK2011	a	*bar1* pDK93A [*GAL1-CLN3::URA*] *rts1Δ::kanMX4*	This study
DK2017	a	*bar1 CLN3-6×HA::HIS*	This study
DK2019	a	*bar1 CLN3-6×HA::HIS rts1Δ::kanMX4*	This study
DK2049	a	*bar1 CLN3-6×HA::HIS rts1Δ::kanMX4 ace2Δ::hphNT1*	This study
DK2053	a	*bar1 CLN2-3×HA::LEU GAL1-YOX1::HIS*	This study
DK2054	a	*bar1 CLN2-3×HA::LEU GAL1-YOX1::HIS rts1Δ::kanMX4*	This study
DK2055	a	*bar1 CLN3-6×HA::HIS ace2Δ::natMX4*	This study
DK2056	a	*bar1 GAL1-CDC20::NatNT2 CLN3-6×HA::HIS*	This study
DK2057	a	*bar1 GAL1-CDC20::NatNT2 CLN3-6×HA::HIS rts1Δ::kanMX4*	This study
DK2058	a	*bar1 GAL1-CDC20::NatNT2 CLN3-6×HA::HIS rts1Δ::kanMX4 ace2Δ::hphNT1*	This study
DK2093	a	*bar1 cbk1Δ::HIS*	This study
DK2136	a	*bar1 GAL1-CDC20::NatNT2 CLN3-6×HA::HIS ace2Δ::kanMX4*	This study
DK2149	a	*bar1 ACE2-GFP::klTRP rts1Δ::kanMX4*	This study
DK2171	a	*bar1 cbk1Δ::HIS rts1Δ::kanMX4*	This study
DK2490	a	*bar1 ACE2-3×HA::kanMX6 cbk1Δ::HIS*	This study
DY150	a		Thomas and Rothstein, 1989
DY151	α		Thomas and Rothstein, 1989
DY3924	α	*ace2Δ::HIS3 lys2*	This study
DY5923	a	*ACE2-MYC(13)::kanMX*	This study
DY8309	a	*ASH1-MYC(13)::kanMX*	Takahata et al., 2011
DY9719	a	*ash1Δ::TRP1 lys2 met15*	This study
DY10788	a	*GAL1-CDC20::ADE2 lys2*	Sbia et al., 2008
DY15549	a	*GAL1-CDC20::ADE2 lys2 ace2::HIS3*	This study
DY15723	α	*rts1Δ::kanMX lys2*	This study
DY15729	α	*ace2Δ::HIS3 rts1Δ::kanMX6 lys2 met15*	This study
DY15995	a	*GAL1-CDC20::ADE2 lys2 rts1::kanMX lys2*	This study
DY15996	a	*GAL1-CDC20::ADE2 lys2 rts1::kanMX ace2::HIS3 lys2*	This study
DY16269	a	*ACE2-MYC(13)::kanMX rts1Δ::hphMX4*	This study
DY16273	a	*ASH1-MYC(13)::kanMX rts1Δ::hphMX4 lys2*	This study
DY17134	a	*GAL1-CDC20::ADE2 yox1::natMX*	This study
DY17236	a	*GAL1-CDC20::ADE2 yox1::natMX ace2Δ::HIS3*	This study
DY17240	a	*GAL1-CDC20::ADE2 yox1::natMX rts1Δ::kanMX*	This study
DY17242	a	*GAL1-CDC20::ADE2 yox1::natMX rts1Δ::kanMX ace2Δ::HIS*	This study
ZZ41	a	*bar1 CLN2-3×HA::LEU2*	Artiles et al., 2009

Ace2 was hyperphosphorylated in newborn daughter cells and underwent gradual dephosphorylation during cell growth, reaching maximal dephosphorylation at approximately the same time that Cln3 protein reached peak levels. This observation suggests the possibility that the extent of Ace2 dephosphorylation could help set the level of *CLN3* transcription.

Cell size checkpoints must translate a parameter related to growth into a proportional checkpoint signal that can be read by downstream components to determine when sufficient growth has occurred. The nature of the proportional checkpoint signal is one of the central enigmas of cell size control. The discovery that Ace2 phosphorylation is proportional to growth suggests that it may respond to a proportional checkpoint signal. Moreover, the central role of $PP2A^{Rts1}$ in control of both Ace2 phosphorylation and cell size suggests that it could be responsible for generating or relaying a proportional checkpoint signal to Ace2, thereby ensuring that Cln3 levels are proportional to growth. $PP2A^{Rts1}$ could also play a role in setting the threshold. In this case, poor nutrients could regulate $PP2A^{Rts1}$ to lower the threshold, thereby allowing cells to go through the cell cycle at a reduced cell size. This kind of model could explain the puzzling observation that cells growing in poor nutrients enter the

cell cycle at a reduced size, despite having reduced levels of Cln3 (Hall et al., 1998; Newcomb et al., 2003). If poor nutrients reduce the threshold, lower levels of Cln3 would be required for cell cycle entry. Further analysis of the targets of $PP2A^{Rts1}$, as well as the signals that control $PP2A^{Rts1}$, will likely provide important new clues to how cell division is linked to cell growth.

Materials and methods

Yeast strains, culture conditions, and plasmids

All strains are in the W303 background (*leu2-3,112 ura3-1 can1-100 ade2-1 his3-11,15 trp1-1 GAL+ ssd1-d2*). The genotypes of the strains used for this study are listed in Table 2. Full-length *CLN3* was expressed from the GAL1 promoter using the integrating plasmid pDK93A (*GAL1-CLN3 URA3*). One-step PCR-based gene replacement was used for construction of deletions and epitope tags at the endogenous locus. Strains that contain *GAL1-CDC20* strains were made by genetic crosses (Bhoite et al., 2001) or by using a PCR-based approach to integrate the *GAL1* promoter in front of the endogenous *CDC20* gene in the appropriate background. Cells were grown in YEPD media (1% yeast extract, 2% peptone, and 2% dextrose) supplemented with 40 mg/liter adenine or in YEP media (1% yeast extract and 2% peptone) supplemented with an added carbon source, as noted.

Preparation of samples for MS

To prepare samples for MS, wild-type and *rts1Δ* cells containing *CLN2-3×HA* were grown in YEPD medium overnight at room temperature. Cells were arrested in G1 with a mating pheromone and released from the arrest at 30°C at an OD_{600} of 0.7. Samples were taken for Cln2-3×HA Western blots every 10 min after the arrest, which were used to confirm that samples for MS were taken just before Cln2 could be detected by Western blotting. At 20 min after release, 25 ml of the culture was harvested by centrifuging 95 s at 3,800 rpm, and 1 ml of ice-cold lysis buffer (8 M urea, 75 mM NaCl, 50 mM Tris-HCl, pH 8.0, 50 mM NaF, 50 mM β-glycerophosphate, 1 mM sodium orthovanadate, 10 mM sodium pyrophosphate, and 1 mM PMSF) was added to the cells and used to transfer them to a wide-bottom, 1.6-ml screw-top tube. The cells were pelleted again, and the supernatant was removed. Approximately 0.5 ml of glass beads was added, and the cells were frozen in liquid nitrogen. The cells were lysed by the addition of 750 µl lysis buffer followed by bead beating using a disrupter (Multibeater-8; BioSpec) at top speed for three cycles of 1 min, each followed by a 1-min incubation on ice to avoid overheating of the lysates. Samples were centrifuged at 13,000 rpm for 15 s, and the supernatants were transferred to fresh 1.6-ml tubes, which were centrifuged at 13,000 rpm for 10 min at 4°C. The supernatants from this spin were transferred to fresh 1.6-ml tubes and frozen in liquid nitrogen. This procedure yielded 0.7 ml of extract at 2–5 mg/ml.

Disulfide bonds were reduced by adding DTT to a final concentration of 2.5 mM and incubating at 56°C for 40 min. The extract was allowed to cool to room temperature, and the reduced cysteines were alkylated by adding iodoacetamide to 7.5 mM and incubating for 40 min in the dark at room temperature. Alkylation was quenched with an additional 5 mM DTT.

Peptide digestion and labeling by reductive dimethylation

Proteins were diluted 2.5-fold into 25 mM (final concentration) Tris-HCl, pH 8.8, and digested by the addition of lysyl endopeptidase (Lys-C; Wako Chemicals USA) to a final concentration of 10 ng/µl with gentle agitation overnight at room temperature. Digested peptides were acidified by the addition of neat formic acid (FA) to a 1% final concentration, and the resultant precipitate was pelleted by centrifuging for 2 min at 21,000 *g*. The supernatants were loaded onto prewet 200 mg tC18, reverse-phase, solid-phase extraction cartridges (Waters). The columns were washed with 6 ml of 1% FA followed by 3 ml phosphate/citrate buffer (227 mM Na_2HPO_4 and 86 mM $NaH_2C_6H_5O_7$, pH 5.5). Peptides were labeled by reductive dimethylation (Boersema et al., 2009) with 6 ml of "light" reductive dimethylation reaction mix (0.8% formaldehyde [Sigma-Aldrich] and 120 mM $NaCNBH_3$ [Sigma-Aldrich] in phosphate/citrate buffer) or with 6 ml of "heavy" reductive dimethylation reaction mix (0.8% D2-formaldehyde [Isotec] and 120 mM $NaCNBD_3$ [C/D/N Isotopes, Inc.] in phosphate/citrate buffer). The columns were washed with 6 ml of 1% FA, and the peptides were eluted with 1 ml of 70% acetonitrile (ACN) and 1% FA. Equal amounts of wild-type (light) and *rts1Δ* (heavy) peptides were combined and dried in a SpeedVac (Savant).

Phosphopeptide enrichment by SCX/TiO_2

Phosphopeptides were enriched using a modified version of the two-step, SCX–immobilized metal affinity chromatography/TiO_2 protocol using step elution from self-packed solid-phase extraction SCX chromatography cartridges as previously described with some changes (Villén and Gygi, 2008; Dephoure and Gygi, 2011). Peptides were resuspended in 1 ml SCX buffer A (7 mM KH_2PO_4, pH 2.65, and 30% ACN) and loaded onto preequilibrated syringe-barrel columns packed with 500 mg of 20-µm, 300-Å PolySULFOETHYL A resin (PolyLC). Peptides were eluted by the sequential addition of 3 ml SCX buffer A containing increasing concentrations of KCl. 12 fractions were collected after elution with 0 (flow through), 10, 20, 30, 40, 50, 60, 70, 80, 90, 100, and 200 mM KCl. All fractions were frozen in liquid nitrogen, lyophilized, resuspended in 1 ml of 1% FA, and desalted on 50-mg Sep-Paks. Peptides were eluted with 500 µl of 70% ACN and 1% FA. 5% of each fraction was taken off for protein abundance analysis. The remaining peptides were dried in a SpeedVac. TiO_2 enrichment was performed by either of two protocols. For replicate one, peptides from fractions 8–11 were pooled after desalting (fraction 12 was not used for phosphopeptide analysis). Dried peptides were resuspended in 50 µl of wash/binding buffer (30% ACN, 1% FA, and 70 mM glutamic acid) and incubated with 500 µg of Titansphere TiO_2 beads (GL Sciences) with vigorous shaking for 60 min at room temperature. The beads were washed three times with 200 µl of wash/binding buffer and once with 1% FA. Phosphopeptides were eluted in two steps by sequential treatments with 50 µl of 0.5-M KH_2PO_4, pH 7.5. The eluates were acidified by the addition of FA to 1% final concentration, desalted on Stage tips (Rappsilber et al., 2003), and dried in a SpeedVac. Eight fractions corresponding to 0, 10, 20, 30, 40, 50, 60, and the pooled 70–100 mM KCl steps were analyzed by LC-MS/MS.

SCX for peptides from replicates 2 and 3 was performed as for set 1, but 11 fractions were taken with steps of 0, 10, 20, 30, 40, 50, 60, 70, 80, 90, and 200 mM KCl. Fractions 9–11 were pooled before TiO_2 enrichment. TiO_2 phosphopeptide enrichment was performed using a modified protocol (Kettenbach and Gerber, 2011) using 2 mg TiO_2 resin for each fraction and a wash/binding buffer composed of 50% ACN and 2 M lactic acid.

MS

Phosphopeptide samples were analyzed on a mass spectrometer (LTQ Orbitrap Velos; Thermo Fisher Scientific) equipped with a quaternary pump (Accela 600; Thermo Fisher Scientific) and a microautosampler (Famos; LC Packings). Nanospray tips were hand pulled using 100-µm inner diameter fused-silica tubing and packed with 0.5 cm of Magic C4 resin (5 µm and 100 Å; Michrom BioResources) followed by 20 cm of Maccel C18AQ resin (3 µm and 200 Å; Nest Group). Peptides were separated using a gradient of 3–28% ACN in 0.125% FA over 70 min with an in-column flow rate of ∼300–500 nl/min.

Peptides were detected using a data-dependent top 20 MS2 method. For each cycle, one full MS scan of mass per charge (m/z) = 300–1,500 was acquired in the Orbitrap at a resolution of 60,000 at m/z = 400 with automatic gain control target = 10^6 and a maximum ion accumulation time of 500 ms. Each full scan was followed by the selection of the most intense ions, up to 20, for collision-induced dissociation and MS2 analysis in the LTQ. An automatic gain control target of 2×10^3 and maximum ion accumulation time of 150 ms were used for MS2 scans. Ions selected for MS2 analysis were excluded from reanalysis for 60 s. Precursor ions with charge = 1 or unassigned were excluded from selection for MS2 analysis. Lock mass, using atmospheric polydimethylsiloxane (m/z = 445.120025) as an internal standard, was used in all runs to calibrate Orbitrap MS precursor masses. For replicate 1, eight fractions were analyzed once each. For replicates 2 and 3, sufficient material was recovered to shoot samples in duplicate for most fractions. For replicate 2, all nine fractions were analyzed in duplicate. For replicate 3, fractions 1–6 were analyzed in duplicate, whereas fractions 7–9 were analyzed once. For protein abundance analysis, 5% of each SCX fraction was removed before phosphopeptide enrichment, desalted on a Stage tip, resuspended in 5% FA, and analyzed in a single run for each fraction as described in the previous paragraphs for phosphopeptides but using a 90-min gradient of 3–25% buffer B and 75-s dynamic exclusion.

Peptide identification and filtering

MS2 spectra were searched using SEQUEST v.28 (revision 13; Eng et al., 1994) against a composite database containing the translated sequences of all predicted open reading frames of *Saccharomyces cerevisiae* (*Saccharomyces* Genome Database, downloaded 10/30/2009) and its reversed complement using the following parameters: a precursor mass tolerance of ±20 ppm; 1.0-D product ion mass tolerance; Lys-C digestion; up to two missed cleavages; static modifications of carbamidomethylation on cysteine (57.0214) and dimethyl adducts (28.0313) on lysine and peptide amino termini; and dynamic modifications for methionine oxidation (15.9949), heavy dimethylation (6.0377) on lysine and peptide amino termini, and phosphate (79.9663) on serine, threonine, and tyrosine for phosphopeptide-enriched samples.

Peptide spectral matches were filtered to a 1% false discovery rate (FDR) using the target decoy strategy (Elias and Gygi, 2007) combined with linear discriminant analysis (Huttlin et al., 2010) using several different parameters, including Xcorr, ΔCn′, precursor mass error, observed ion charge state, and predicted solution charge state. Linear discriminant models were calculated for each LC-MS/MS run using peptide matches to forward and reversed protein sequences as positive and negative training data. Peptide spectral matches within each run were sorted in descending order by a discriminant score and filtered to a 1% FDR as revealed by the number of decoy sequences remaining in the dataset. The data were further filtered to control protein level FDRs. Peptides from all fractions in each experiment were combined and assembled into proteins. Protein scores were derived from the product of all linear discriminant analysis peptide probabilities, sorted by rank, and filtered to 1% FDR as described for peptides. The FDR of the remaining peptides fell dramatically after protein filtering. Remaining peptide matches to the decoy database were removed from the final dataset.

For inclusion in quantitative calculations, peptides were required to have a minimum signal-to-noise ratio of ≥5 or a maximum value ≥10 for heavy and light species. Protein abundance ratios were calculated using the median $\log_2$ ratio of all peptides for each protein. This was performed independently for each of the three biological replicate experiments, and only those proteins for which we quantified more than two unique peptides were retained in the dataset (Table S1). Ratios were normalized to recenter the distribution at 1:1 ($\log_2 = 0$). Phosphopeptide ratios were adjusted for changes in protein abundance where possible using the corresponding protein ratio from the matched experiment. However, corrections were only applied if protein levels were available for all experiments in which the phosphosite was quantified (7,230 of 9,255 quantified sites were corrected for protein level abundance and 3,983 of 5,159 high quality sites quantified in two or more replicates). We note that although we were unable to normalize all phosphorylation site quantifications to protein level changes, the vast majority of proteins undergo almost no change in abundance between the two samples ($\log_2$ ratio SD = 0.32); thus, most uncorrected ratios are unlikely to be significantly skewed. Phosphorylation site ratios were calculated from the median of all quantified phosphopeptides harboring each site in each replicate.

Phosphorylation site localization analysis was performed using the Ascore algorithm (Beausoleil et al., 2006). These values appear in Table S2.

Cell cycle time courses and log phase cells

To ensure that protein loading was normalized in time course experiments, we determined ODs of cultures from each strain that yield equal amounts of extracted protein. This was necessary because large cells (i.e., *rts1Δ* cells) or clumpy cells (i.e., *ace2Δ* cells) scatter light differently. Samples of cultures from each strain at varying ODs were harvested, and the cells were lysed by bead beating. The protein concentration in extracts from each strain was then measured to determine which ODs yield comparable amounts of extracted protein. We found that ODs of 0.6 (wild type), 0.8 (*rts1Δ*), 0.5 (*ace2Δ*), and 0.5 (*rts1Δ ace2Δ*) yielded protein concentrations with differences of less than twofold. We also used multiple background bands in Western blots to ensure that protein loading between strains and individual samples was normalized.

To synchronize cells in G1 with a mating pheromone, cells were grown to log phase in YEPD overnight at room temperature before synchronization. Cells at an OD_{600} of 0.6 were arrested in G1 by addition of 0.5 µg/ml of α factor for 3.5 h at room temperature. Cells were released into a synchronous cell cycle by washing 3× with fresh YEPD prewarmed to 30°C. Time courses were performed at 30°C unless otherwise noted. To prevent cells from reentering the cell cycle, α factor was added back at 65 min after release.

To synchronize cells at metaphase, cells containing *GAL1-CDC20* were grown overnight in YEP media containing 2% raffinose and 2% galactose. Cells were arrested by washing into media containing 2% raffinose and incubated at room temperature for 4 h. Cells were released from the metaphase arrest by adding 2% galactose and were then shifted to 30°C for Western blotting experiments or 25°C for *CLN3* mRNA analysis.

For induced expression experiments, cells were grown overnight in YEP medium containing 2% glycerol and 2% ethanol. Expression of genes from the *GAL1* promoter was induced by addition of 2% galactose, and the cells were shifted to 30°C.

For time courses using analogue-sensitive alleles, cells were grown overnight in YEPD without adenine. The adenine analogue inhibitor 1NM-PP1 was added to log phase cells at a final concentration of 25 µM, and the cells were then shifted to 30°C.

To analyze log phase cells, cultures were grown in YEPD, YEPD + 2% galactose, or YEPD + 2% glycerol/ethanol overnight at room temperature. 1.6 ml of cells at an OD_{600} of 0.6 were collected and centrifuged at 13,000 rpm for 30 s, the supernatant was removed, and 250 µl of glass beads were added before freezing in liquid nitrogen.

Western blotting

To collect samples for Western blotting, 1.6-ml samples were collected at each time point and centrifuged at 13,000 rpm for 30 s. The supernatant was removed, and 250 µl of glass beads were added before freezing in liquid nitrogen. Cells were lysed using 140 µl of sample buffer (65 mM Tris-HCl, pH 6.8, 3% SDS, 10% glycerol, 50 mM NaF, 100 mM β-glycerophosphate, 5% 2-mercaptoethanol, and bromophenol blue). PMSF was added to the sample buffer to 2 mM immediately before use. Cells were lysed in a Multibeater-8 at top speed for 2 min. The samples were removed and centrifuged for 15 s at 13,000 rpm in a microfuge and placed in boiling water for 5 min. After boiling, the samples were centrifuged for 5 min at 13,000 rpm and loaded on an SDS polyacrylamide gel.

To assay phosphorylation of Ace2 serine 122, cells were grown overnight in YEPD media at room temperature to OD_{600} = 0.6. Cells from 50 ml of culture were pelleted, resuspended in 1 ml of ice-cold 50 mM Hepes, pH 7.6, and pelleted in a wide-bottomed 1.6-ml screw top tube. Cells were lysed by bead beating in 600 µl lysis buffer (50 mM Tris-HCl, pH 7.5,150 mM NaCl,1% Triton X-100, 10% glycerol, 120 mM β-glycerophosphate, and 2 mM sodium orthovanadate) containing 2 mM PMSF, 1 mM leupeptin, 1 mM chymostatin, 1 mM pepstatin, and 20 µM cantharidin. Ace2-3×HA was immunoprecipitated with mouse monoclonal 12CA5 antibody. Western blots were probed with rabbit anti–phospho-S122 antibody (gift of E. Weiss, Northwestern University, Evanston, IL) as previously described, except that the antibody was used at a dilution of 1:30,000 in TBST (10 mM Tris-Cl, pH 7.5, 100 mM NaCl, and 0.1% Tween 20) containing 4% BSA (Mazanka and Weiss, 2010).

SDS-PAGE was performed as previously described (Harvey et al., 2005). Gels were run at a constant current of 20 mA. For Ace2, Clb2, and Cln3, electrophoresis was performed on 10% polyacrylamide gels until a 29-kD prestained marker ran to the bottom of the gel. Protein was transferred to nitrocellulose membranes for 1.5 h at 800 mA at 4°C in a transfer tank (TE22; Hoeffer) in buffer containing 20 mM Tris base, 150 mM glycine, and 20% methanol. Blots were probed overnight at 4°C with affinity-purified rabbit polyclonal antibodies raised against Ace2, Clb2, or the HA peptide or mouse monoclonal antibody against the HA peptide. Cln3-6×HA blots were probed with the 12CA5 anti-HA monoclonal antibody. All blots were probed with an HRP-conjugated donkey anti–rabbit secondary antibody (GE Healthcare) or HRP-conjugated donkey anti–mouse antibody for 45–90 min at room temperature. Secondary antibodies were detected via chemiluminescence with Advansta ECL or Quantum reagents.

RNA analysis

qRT-PCR was used to measure *CLN3* mRNA levels as described using RPR1 RNA as the internal control (*CLN3* primers: 5′-CAGCGATCAGCGAATACAATAA-3′ and 5′-TGATAATGAACCGCGAGGAA-3′; *RPR1* control primers: 5′-CACCTATGGGCGGGTTATCAG-3′ and 5′-CCTAGGCCGAACTCCGTGA-3′; Voth et al., 2007). Northern blotting probes for *CLN3* and *ACT1* RNA were made using gel-purified PCR products (*CLN3* oligonucleotides: 5′-GCGGGATCCATGGCCATATTGAAGGATAC-3′ and 5′-GCGGAGCTCTCAGCGAGTTTTCTTGAGGT-3′; *ACT1* oligonucleotides: 5′-TCATACCTTCTACAACGAATTGAGA-3′ and 5′-ACACTTCATGATGGAGTTGTAAGT-3′). Probes were labeled using the DNA labeling kit (Megaprime; GE Healthcare). RNA for Northern blotting was isolated as previously described (Cross and Tinkelenberg, 1991; Kellogg and Murray,

1995). In brief, 1.6-ml samples were collected at each time point and centrifuged for 30 s at 13,000 rpm. The supernatant was removed, and 200 µl of acid-washed beads was added before freezing in liquid nitrogen. 350 µl NETS buffer (0.3 M NaCl, 1 mM EDTA, 10 mM Tris-HCl, pH 7.5, and 0.2% SDS) and 350 µl phenol/chloroform were added to each cell pellet, and cells were lysed by shaking in a Multibeater-8 at full speed for 2 min. Samples were then centrifuged at 15,000 *g* for 5 min, and 300 µl of the aqueous phase was transferred to a new tube. RNA was ethanol precipitated and resuspended in TE buffer (10 mM Tris-HCl, pH 7.5, and 1 mM EDTA) containing 0.2% SDS followed by incubation at 65°C for 10 min. The samples were run in a 1% formaldehyde-agarose gel at 5 V/cm^2. The same fraction of total extracted RNA was loaded at each time point. This typically corresponded to 8 µg RNA at the 0 time point. *CLN3* blots were stripped and reprobed for *ACT1* to control for loading.

ChIP assays

ChIPs were performed as previously described (Voth et al., 2007). Yeast cells were collected at an OD of 0.6–0.8 and cross-linked in 1% formaldehyde for 20 min at room temperature. Cross-linking was quenched with 0.125 M glycine for 5 min, and cells were washed twice with TBS. Cell pellets were resuspended in lysis buffer (0.1% deoxycholic acid, 1 mM EDTA, 50 mM Hepes, pH 7.5, 140 mM NaCl, and 1% Triton X-100 supplemented with 0.8 mM DTT and protease inhibitors) and were lysed with 0.5-mm zirconia beads (BioSpec) in a cell disrupter (Mini-Beadbeater; BioSpec). After centrifugation, the pellet was washed with lysis buffer and sonicated to a shearing size of <500 nucleotides using a bath sonicator (Biorupter XL; Diagenode). The sonicated material was centrifuged, and the supernatant containing the chromatin was quantitated by Bradford assay.

Immunoprecipitations were performed overnight at 4°C using 500–700 µg of chromatin, 4A6 monoclonal antibody to the Myc epitope (EMD Millipore), and Pan–Mouse Dyna Beads IgG (Invitrogen). The beads were washed twice with lysis buffer, twice with high salt buffer (lysis buffer with 500 mM NaCl), twice with LiCl buffer (0.5% deoxycholic acid, 1 mM EDTA, 250 mM LiCl, 0.5% NP-40, and 10 mM Tris-HCl, pH 8.0), and once with TE. Cross-links were reversed overnight in elution buffer (10 mM EDTA, 1% SDS, and 50 mM Tris-HCl, pH 8.0) at 65°C. DNA was purified using the PCR purification kit (QIAquick; QIAGEN). Quantitative PCR reactions were performed using a detection system (LightCycler480 II; Roche). A standard curve representing a range of concentrations of input samples was used for quantitating the amount of product for each sample with each primer set. All ChIP samples were normalized to corresponding input control samples, to a genomic reference region on chromosome I, and to a genetically identical untagged strain as a control. (ChIP primers for the *CLN3* promoter region: 5′-TACATTCTGTGCTGGCGACC-3′, 5′-TTTGAGCACAGCGTTTGGTTG-3′, 5′-ATTCGTCTCGTTTGAAC-GCTTG-3′, and 5′-GCCAAGCGTTCAAACGAGAC-3′; ChIP primers for the chromosome I control region: 5′-GTTTATAGCGGGCATTATGCGTAGATCAG-3′ and 5′-GTTCCTCTAGAATTTTTCCACTCGCACATTC-3′).

Analysis of cell size, bud emergence, and cell proliferation

Triplicate cell cultures were grown overnight to log phase at room temperature in YEPD or YEP containing 2% galactose. A 0.9-ml sample of each culture was fixed with 100 µl of 37% formaldehyde for 1 h and then washed twice with PBS + 0.04% sodium azide + 0.02% Tween 20. Cell size was measured using a Coulter counter (Channelizer Z2; Beckman Coulter) as previously described (Jorgensen et al., 2002). In brief, 150 µl of fixed culture was diluted in 20 ml diluent (Isoton II; Beckman Coulter) and sonicated for 20 s before cell sizing. Each plot is the average of three independent experiments in which three independent samples were analyzed per strain. The size of elutriated cells was measured in the same manner except that the cells were not sonicated. The percentage of budded cells was measured by counting the number of small unbudded cells over a total of ≥200 cells using a phase-contrast microscope (Carl Zeiss) with a 40×/0.65 NA objective (Carl Zeiss).

To assay the rate of cell proliferation on plates, cells were grown overnight in YEPD at room temperature and adjusted to an OD_{600} of 1.0. Fivefold serial dilutions were spotted onto YEPD or YEP containing 2% galactose and incubated at 30 or 37°C. To assay the growth rate in liquid cultures, eight independent cultures of each strain were grown overnight, and each was diluted 100-fold in inoculating 0.2-ml cultures in a 100-well plate where growth was monitored in a Bioscreen C apparatus (Growth Curves USA).

Immunoaffinity purifications and in vitro assays

Immunoaffinity purification of Ace2-3×HA and Cbk1-3×HA was performed in the presence of 1 M KCl as previously described with the following changes (Mortensen et al., 2002). Affinity beads were prepared by binding 0.6 mg anti-HA antibody to 0.5 ml protein A beads overnight at 4°C. 14 g of frozen cell powder was resuspended in 30 ml lysis buffer (50 mM Hepes-KOH, pH 7.6, 1 M KCL, 1 mM EGTA, 1 mM $MgCl_2$, 0.25% Tween 20, and 5% glycerol) containing 1 mM PMSF by stirring at 4°C for 15 min. The cell extract was centrifuged at 40,000 rpm for 1 h. The elution buffer contained 50 mM Hepes-KOH, pH 7.6, 250 mM KCl, 1 mM EGTA, 1 mM $MgCl_2$, 5% glycerol, and 0.5 mg/ml HA dipeptide. The Ace2-3×HA was treated with λ phosphatase before elution.

To test whether Cbk1 directly phosphorylates Ace2, purified Ace2 and Cbk1 were mixed in the presence of 1 mM ATP and kinase assay buffer (50 mM Hepes-KOH, pH 7.6, 1 mM $MgCl_2$, 1 mM DTT, 5% glycerol, 0.05% Tween 20, and 10 ng/µl BSA). The reactions were incubated for 30 min at 30°C and then quenched with 4× SDS-PAGE sample buffer (260 mM Tris-HCl, pH 6.8, 12% SDS, 40% glycerol, and 0.04% bromophenol blue). The samples were loaded onto a 10% SDS-PAGE gel, which was transferred to nitrocellulose and probed with anti-Ace2. Similar approaches were used to test the effects of purified Cdk1/Clb2 (Harvey et al., 2011).

Centrifugal elutriation

Cells for elutriation were grown overnight at 30°C in YEP medium containing 2% glycerol and 2% ethanol to increase the fraction of very small unbudded cells. Centrifugal elutriation was performed as previously described (Futcher, 1999; McCusker et al., 2012). In brief, cells were elutriated at 4°C in a centrifuge (J6-MI; Beckman Coulter) with a rotor (JE-5.0; Beckman Coulter) at 2,700 rpm. Small unbudded cells were released into fresh YEPD media at 25°C, and samples were taken at 10-min intervals.

Online supplemental material

Fig. S1 shows an example of phosphopeptide quantification data obtained by proteome-wide MS. Fig. S2 shows loading controls for Fig. 6 (A, C, and D). Table S1 lists relative protein abundance measurements for all quantified proteins, including average values as well as those for each biological replicate. Table S2 lists all sites detected by MS listed by protein and site along with quantification data for all three replicates. Table S3 lists all phosphopeptides that passed peptide and protein target decoy filtering along with key SEQUEST search parameters and Ascore site localization data. Table S4 lists all sites that showed significantly increased phosphorylation in *rts1Δ* cells. Table S5 lists all sites that showed significantly decreased phosphorylation in *rts1Δ* cells. Online supplemental material is available at http://www.jcb.org/cgi/content/full/jcb.201309119/DC1.

We thank members of the laboratory for advice and support and Vu Thai for help with protein purification and in vitro assays. We also thank Eric Weiss for the Ace2 phosphospecific antibody.

This work was supported by National Institutes of Health grant GM053959 (D. Kellogg) and National Institutes of Health grant GM39067 (D. Stillman).

The authors declare no competing financial interests.

Submitted: 24 September 2013
Accepted: 12 December 2013

References

Aerne, B.L., A.L. Johnson, J.H. Toyn, and L.H. Johnston. 1998. Swi5 controls a novel wave of cyclin synthesis in late mitosis. *Mol. Biol. Cell.* 9:945–956. http://dx.doi.org/10.1091/mbc.9.4.945

Altman, R., and D.R. Kellogg. 1997. Control of mitotic events by Nap1 and the Gin4 kinase. *J. Cell Biol.* 138:119–130. http://dx.doi.org/10.1083/jcb.138.1.119

Artiles, K., S. Anastasia, D. McCusker, and D.R. Kellogg. 2009. The Rts1 regulatory subunit of protein phosphatase 2A is required for control of G1 cyclin transcription and nutrient modulation of cell size. *PLoS Genet.* 5:e1000727. http://dx.doi.org/10.1371/journal.pgen.1000727

Barral, Y., M. Parra, S. Bidlingmaier, and M. Snyder. 1999. Nim1-related kinases coordinate cell cycle progression with the organization of the peripheral cytoskeleton in yeast. *Genes Dev.* 13:176–187. http://dx.doi.org/10.1101/gad.13.2.176

Bastajian, N., H. Friesen, and B.J. Andrews. 2013. Bck2 acts through the MADS box protein Mcm1 to activate cell-cycle-regulated genes in budding

yeast. *PLoS Genet.* 9:e1003507. http://dx.doi.org/10.1371/journal.pgen.1003507

Beausoleil, S.A., J. Villén, S.A. Gerber, J. Rush, and S.P. Gygi. 2006. A probability-based approach for high-throughput protein phosphorylation analysis and site localization. *Nat. Biotechnol.* 24:1285–1292. http://dx.doi.org/10.1038/nbt1240

Belenguer, P., L. Pelloquin, M.L. Oustrin, and B. Ducommun. 1997. Role of the fission yeast nim 1 protein kinase in the cell cycle response to nutritional signals. *Biochem. Biophys. Res. Commun.* 232:204–208. http://dx.doi.org/10.1006/bbrc.1997.6253

Bhoite, L.T., Y. Yu, and D.J. Stillman. 2001. The Swi5 activator recruits the Mediator complex to the HO promoter without RNA polymerase II. *Genes Dev.* 15:2457–2469. http://dx.doi.org/10.1101/gad.921601

Bishop, A.C., J.A. Ubersax, D.T. Petsch, D.P. Matheos, N.S. Gray, J. Blethrow, E. Shimizu, J.Z. Tsien, P.G. Schultz, M.D. Rose, et al. 2000. A chemical switch for inhibitor-sensitive alleles of any protein kinase. *Nature*. 407:395–401. http://dx.doi.org/10.1038/35030148

Bobola, N., R.P. Jansen, T.H. Shin, and K. Nasmyth. 1996. Asymmetric accumulation of Ash1p in postanaphase nuclei depends on a myosin and restricts yeast mating-type switching to mother cells. *Cell*. 84:699–709. http://dx.doi.org/10.1016/S0092-8674(00)81048-X

Boersema, P.J., R. Raijmakers, S. Lemeer, S. Mohammed, and A.J. Heck. 2009. Multiplex peptide stable isotope dimethyl labeling for quantitative proteomics. *Nat. Protoc.* 4:484–494. http://dx.doi.org/10.1038/nprot.2009.21

Breeden, L., and G.E. Mikesell. 1991. Cell cycle-specific expression of the SWI4 transcription factor is required for the cell cycle regulation of HO transcription. *Genes Dev.* 5:1183–1190. http://dx.doi.org/10.1101/gad.5.7.1183

Caplan, A.J., and M.G. Douglas. 1991. Characterization of YDJ1: a yeast homologue of the bacterial dnaJ protein. *J. Cell Biol.* 114:609–621. http://dx.doi.org/10.1083/jcb.114.4.609

Chan, L.Y., and A. Amon. 2009. The protein phosphatase 2A functions in the spindle position checkpoint by regulating the checkpoint kinase Kin4. *Genes Dev.* 23:1639–1649. http://dx.doi.org/10.1101/gad.1804609

Colman-Lerner, A., T.E. Chin, and R. Brent. 2001. Yeast Cbk1 and Mob2 activate daughter-specific genetic programs to induce asymmetric cell fates. *Cell*. 107:739–750. http://dx.doi.org/10.1016/S0092-8674(01)00596-7

Cross, F.R. 1988. DAF1, a mutant gene affecting size control, pheromone arrest, and cell cycle kinetics of *Saccharomyces cerevisiae*. *Mol. Cell. Biol.* 8:4675–4684.

Cross, F.R. 1990. Cell cycle arrest caused by CLN gene deficiency in *Saccharomyces cerevisiae* resembles START-I arrest and is independent of the mating-pheromone signalling pathway. *Mol. Cell. Biol.* 10:6482–6490.

Cross, F.R., and A.H. Tinkelenberg. 1991. A potential positive feedback loop controlling CLN1 and CLN2 gene expression at the start of the yeast cell cycle. *Cell*. 65:875–883. http://dx.doi.org/10.1016/0092-8674(91)90394-E

Dephoure, N., and S.P. Gygi. 2011. A solid phase extraction-based platform for rapid phosphoproteomic analysis. *Methods*. 54:379–386. http://dx.doi.org/10.1016/j.ymeth.2011.03.008

Di Como, C.J., H. Chang, and K.T. Arndt. 1995. Activation of CLN1 and CLN2 G1 cyclin gene expression by BCK2. *Mol. Cell. Biol.* 15:1835–1846.

Dirick, L., and K. Nasmyth. 1991. Positive feedback in the activation of G1 cyclins in yeast. *Nature*. 351:754–757. http://dx.doi.org/10.1038/351754a0

Di Talia, S., J.M. Skotheim, J.M. Bean, E.D. Siggia, and F.R. Cross. 2007. The effects of molecular noise and size control on variability in the budding yeast cell cycle. *Nature*. 448:947–951. http://dx.doi.org/10.1038/nature06072

Di Talia, S., H. Wang, J.M. Skotheim, A.P. Rosebrock, B. Futcher, and F.R. Cross. 2009. Daughter-specific transcription factors regulate cell size control in budding yeast. *PLoS Biol.* 7:e1000221. http://dx.doi.org/10.1371/journal.pbio.1000221

Dohrmann, P.R., G. Butler, K. Tamai, S. Dorland, J.R. Greene, D.J. Thiele, and D.J. Stillman. 1992. Parallel pathways of gene regulation: homologous regulators SWI5 and ACE2 differentially control transcription of HO and chitinase. *Genes Dev.* 6:93–104. http://dx.doi.org/10.1101/gad.6.1.93

Doolin, M.T., A.L. Johnson, L.H. Johnston, and G. Butler. 2001. Overlapping and distinct roles of the duplicated yeast transcription factors Ace2p and Swi5p. *Mol. Microbiol.* 40:422–432. http://dx.doi.org/10.1046/j.1365-2958.2001.02388.x

Elias, J.E., and S.P. Gygi. 2007. Target-decoy search strategy for increased confidence in large-scale protein identifications by mass spectrometry. *Nat. Methods*. 4:207–214. http://dx.doi.org/10.1038/nmeth1019

Eng, J.K., A.L. McCormack, and J.R. Yates III. 1994. An approach to correlate tandem mass spectral data of peptides with amino acid sequences in a protein database. *J. Am. Soc. Mass Spectrom.* 5:976–989. http://dx.doi.org/10.1016/1044-0305(94)80016-2

Ferrezuelo, F., N. Colomina, A. Palmisano, E. Garí, C. Gallego, A. Csikász-Nagy, and M. Aldea. 2012. The critical size is set at a single-cell level by growth rate to attain homeostasis and adaptation. *Nat Commun*. 3:1012. http://dx.doi.org/10.1038/ncomms2015

Futcher, B. 1999. Cell cycle synchronization. *Methods Cell Sci.* 21:79–86. http://dx.doi.org/10.1023/A:1009872403440

Gould, K.L., and P. Nurse. 1989. Tyrosine phosphorylation of the fission yeast $cdc2^{+}$ protein kinase regulates entry into mitosis. *Nature*. 342:39–45. http://dx.doi.org/10.1038/342039a0

Hadwiger, J.A., C. Wittenberg, H.E. Richardson, M. de Barros Lopes, and S.I. Reed. 1989. A family of cyclin homologs that control the G1 phase in yeast. *Proc. Natl. Acad. Sci. USA*. 86:6255–6259. http://dx.doi.org/10.1073/pnas.86.16.6255

Hall, D.D., D.D. Markwardt, F. Parviz, and W. Heideman. 1998. Regulation of the Cln3-Cdc28 kinase by cAMP in *Saccharomyces cerevisiae*. *EMBO J.* 17:4370–4378. http://dx.doi.org/10.1093/emboj/17.15.4370

Hartwell, L.H., and M.W. Unger. 1977. Unequal division in *Saccharomyces cerevisiae* and its implications for the control of cell division. *J. Cell Biol.* 75:422–435. http://dx.doi.org/10.1083/jcb.75.2.422

Harvey, S.L., and D.R. Kellogg. 2003. Conservation of mechanisms controlling entry into mitosis: budding yeast wee1 delays entry into mitosis and is required for cell size control. *Curr. Biol.* 13:264–275. http://dx.doi.org/10.1016/S0960-9822(03)00049-6

Harvey, S.L., A. Charlet, W. Haas, S.P. Gygi, and D.R. Kellogg. 2005. Cdk1-dependent regulation of the mitotic inhibitor Wee1. *Cell*. 122:407–420. http://dx.doi.org/10.1016/j.cell.2005.05.029

Harvey, S.L., G. Enciso, N.E. Dephoure, S.P. Gygi, J. Gunawardena, and D.R. Kellogg. 2011. A phosphatase threshold sets the level of Cdk1 activity in early mitosis in budding yeast. *Mol. Biol. Cell*. 22:3595–3608. http://dx.doi.org/10.1091/mbc.E11-04-0340

Huttlin, E.L., M.P. Jedrychowski, J.E. Elias, T. Goswami, R. Rad, S.A. Beausoleil, J. Villén, W. Haas, M.E. Sowa, and S.P. Gygi. 2010. A tissue-specific atlas of mouse protein phosphorylation and expression. *Cell*. 143:1174–1189. http://dx.doi.org/10.1016/j.cell.2010.12.001

Janssens, V., and J. Goris. 2001. Protein phosphatase 2A: a highly regulated family of serine/threonine phosphatases implicated in cell growth and signalling. *Biochem. J.* 353:417–439. http://dx.doi.org/10.1042/0264-6021:3530417

Johnston, G.C., J.R. Pringle, and L.H. Hartwell. 1977. Coordination of growth with cell division in the yeast *Saccharomyces cerevisiae*. *Exp. Cell Res.* 105:79–98. http://dx.doi.org/10.1016/0014-4827(77)90154-9

Jorgensen, P., and M. Tyers. 2004. How cells coordinate growth and division. *Curr. Biol.* 14:R1014–R1027. http://dx.doi.org/10.1016/j.cub.2004.11.027

Jorgensen, P., J.L. Nishikawa, B.J. Breitkreutz, and M. Tyers. 2002. Systematic identification of pathways that couple cell growth and division in yeast. *Science*. 297:395–400. http://dx.doi.org/10.1126/science.1070850

Jorgensen, P., I. Rupes, J.R. Sharom, L. Schneper, J.R. Broach, and M. Tyers. 2004. A dynamic transcriptional network communicates growth potential to ribosome synthesis and critical cell size. *Genes Dev.* 18:2491–2505. http://dx.doi.org/10.1101/gad.1228804

Kellogg, D.R. 2003. Wee1-dependent mechanisms required for coordination of cell growth and cell division. *J. Cell Sci.* 116:4883–4890. http://dx.doi.org/10.1242/jcs.00908

Kellogg, D.R., and A.W. Murray. 1995. NAP1 acts with Clb1 to perform mitotic functions and to suppress polar bud growth in budding yeast. *J. Cell Biol.* 130:675–685. http://dx.doi.org/10.1083/jcb.130.3.675

Kettenbach, A.N., and S.A. Gerber. 2011. Rapid and reproducible single-stage phosphopeptide enrichment of complex peptide mixtures: application to general and phosphotyrosine-specific phosphoproteomics experiments. *Anal. Chem.* 83:7635–7644. http://dx.doi.org/10.1021/ac201894j

Laabs, T.L., D.D. Markwardt, M.G. Slattery, L.L. Newcomb, D.J. Stillman, and W. Heideman. 2003. ACE2 is required for daughter cell-specific G1 delay in *Saccharomyces cerevisiae*. *Proc. Natl. Acad. Sci. USA*. 100:10275–10280. http://dx.doi.org/10.1073/pnas.1833999100

Longtine, M.S., C.L. Theesfeld, J.N. McMillan, E. Weaver, J.R. Pringle, and D.J. Lew. 2000. Septin-dependent assembly of a cell cycle-regulatory module in *Saccharomyces cerevisiae*. *Mol. Cell. Biol.* 20:4049–4061. http://dx.doi.org/10.1128/MCB.20.11.4049-4061.2000

Ma, X.J., Q. Lu, and M. Grunstein. 1996. A search for proteins that interact genetically with histone H3 and H4 amino termini uncovers novel regulators of the Swe1 kinase in *Saccharomyces cerevisiae*. *Genes Dev.* 10:1327–1340. http://dx.doi.org/10.1101/gad.10.11.1327

Mazanka, E., and E.L. Weiss. 2010. Sequential counteracting kinases restrict an asymmetric gene expression program to early G1. *Mol. Biol. Cell*. 21:2809–2820. http://dx.doi.org/10.1091/mbc.E10-02-0174

Mazanka, E., J. Alexander, B.J. Yeh, P. Charoenpong, D.M. Lowery, M. Yaffe, and E.L. Weiss. 2008. The NDR/LATS family kinase Cbk1 directly

controls transcriptional asymmetry. *PLoS Biol.* 6:e203. http://dx.doi.org/10.1371/journal.pbio.0060203

McCusker, D., C. Denison, S. Anderson, T.A. Egelhofer, J.R. Yates III, S.P. Gygi, and D.R. Kellogg. 2007. Cdk1 coordinates cell-surface growth with the cell cycle. *Nat. Cell Biol.* 9:506–515. http://dx.doi.org/10.1038/ncb1568

McCusker, D., A. Royou, C. Velours, and D. Kellogg. 2012. Cdk1-dependent control of membrane-trafficking dynamics. *Mol. Biol. Cell*. 23:3336–3347. http://dx.doi.org/10.1091/mbc.E11-10-0834

McMillan, J.N., M.S. Longtine, R.A.L. Sia, C.L. Theesfeld, E.S.G. Bardes, J.R. Pringle, and D.J. Lew. 1999. The morphogenesis checkpoint in *Saccharomyces cerevisiae*: cell cycle control of Swe1p degradation by Hsl1p and Hsl7p. *Mol. Cell. Biol.* 19:6929–6939.

Moffat, J., and B. Andrews. 2004. Late-G1 cyclin-CDK activity is essential for control of cell morphogenesis in budding yeast. *Nat. Cell Biol.* 6:59–66. http://dx.doi.org/10.1038/ncb1078

Mortensen, E.M., H. McDonald, J. Yates III, and D.R. Kellogg. 2002. Cell cycle-dependent assembly of a Gin4-septin complex. *Mol. Biol. Cell*. 13:2091–2105. http://dx.doi.org/10.1091/mbc.01-10-0500

Nash, R., G. Tokiwa, S. Anand, K. Erickson, and A.B. Futcher. 1988. The WHI1+ gene of *Saccharomyces cerevisiae* tethers cell division to cell size and is a cyclin homolog. *EMBO J.* 7:4335–4346.

Nasmyth, K., and L. Dirick. 1991. The role of SWI4 and SWI6 in the activity of G1 cyclins in yeast. *Cell*. 66:995–1013. http://dx.doi.org/10.1016/0092-8674(91)90444-4

Newcomb, L.L., J.A. Diderich, M.G. Slattery, and W. Heideman. 2003. Glucose regulation of *Saccharomyces cerevisiae* cell cycle genes. *Eukaryot. Cell*. 2:143–149. http://dx.doi.org/10.1128/EC.2.1.143-149.2003

Nurse, P. 1975. Genetic control of cell size at cell division in yeast. *Nature*. 256:547–551. http://dx.doi.org/10.1038/256547a0

O'Conalláin, C., M.T. Doolin, C. Taggart, F. Thornton, and G. Butler. 1999. Regulated nuclear localisation of the yeast transcription factor Ace2p controls expression of chitinase (CTS1) in *Saccharomyces cerevisiae*. *Mol. Gen. Genet.* 262:275–282. http://dx.doi.org/10.1007/s004380051084

Ogas, J., B.J. Andrews, and I. Herskowitz. 1991. Transcriptional activation of CLN1, CLN2, and a putative new G1 cyclin (HCS26) by SWI4, a positive regulator of G1-specific transcription. *Cell*. 66:1015–1026. http://dx.doi.org/10.1016/0092-8674(91)90445-5

Okuzaki, D., T. Watanabe, S. Tanaka, and H. Nojima. 2003. The *Saccharomyces cerevisiae* bud-neck proteins Kcc4 and Gin4 have distinct but partially-overlapping cellular functions. *Genes Genet. Syst.* 78:113–126. http://dx.doi.org/10.1266/ggs.78.113

Polymenis, M., and E.V. Schmidt. 1997. Coupling of cell division to cell growth by translational control of the G1 cyclin CLN3 in yeast. *Genes Dev.* 11:2522–2531. http://dx.doi.org/10.1101/gad.11.19.2522

Pramila, T., S. Miles, D. GuhaThakurta, D. Jemiolo, and L.L. Breeden. 2002. Conserved homeodomain proteins interact with MADS box protein Mcm1 to restrict ECB-dependent transcription to the M/G1 phase of the cell cycle. *Genes Dev.* 16:3034–3045. http://dx.doi.org/10.1101/gad.1034302

Rappsilber, J., Y. Ishihama, and M. Mann. 2003. Stop and go extraction tips for matrix-assisted laser desorption/ionization, nanoelectrospray, and LC/MS sample pretreatment in proteomics. *Anal. Chem.* 75:663–670. http://dx.doi.org/10.1021/ac026117i

Richardson, H.E., C.W. Wittenberg, F. Cross, and S.I. Reed. 1989. An essential G1 function for cyclin-like proteins in yeast. *Cell*. 59:1127–1133. http://dx.doi.org/10.1016/0092-8674(89)90768-X

Russell, P., and P. Nurse. 1987. Negative regulation of mitosis by wee1+, a gene encoding a protein kinase homolog. *Cell*. 49:559–567. http://dx.doi.org/10.1016/0092-8674(87)90458-2

Sbia, M., E.J. Parnell, Y. Yu, A.E. Olsen, K.L. Kretschmann, W.P. Voth, and D.J. Stillman. 2008. Regulation of the yeast Ace2 transcription factor during the cell cycle. *J. Biol. Chem.* 283:11135–11145. http://dx.doi.org/10.1074/jbc.M800196200

Shulewitz, M.J., C.J. Inouye, and J. Thorner. 1999. Hsl7 localizes to a septin ring and serves as an adapter in a regulatory pathway that relieves tyrosine phosphorylation of Cdc28 protein kinase in *Saccharomyces cerevisiae*. *Mol. Cell. Biol.* 19:7123–7137.

Sreenivasan, A., and D. Kellogg. 1999. The elm1 kinase functions in a mitotic signaling network in budding yeast. *Mol. Cell. Biol.* 19:7983–7994.

Takahata, S., Y. Yu, and D.J. Stillman. 2011. Repressive chromatin affects factor binding at yeast HO (homothallic switching) promoter. *J. Biol. Chem.* 286:34809–34819. http://dx.doi.org/10.1074/jbc.M111.281626

Thomas, B.J., and R. Rothstein. 1989. Elevated recombination rates in transcriptionally active DNA. *Cell*. 56:619–630. http://dx.doi.org/10.1016/0092-8674(89)90584-9

Turner, J.J., J.C. Ewald, and J.M. Skotheim. 2012. Cell size control in yeast. *Curr. Biol.* 22:R350–R359. http://dx.doi.org/10.1016/j.cub.2012.02.041

Tyers, M., G. Tokiwa, R. Nash, and B. Futcher. 1992. The Cln3-Cdc28 kinase complex of *S. cerevisiae* is regulated by proteolysis and phosphorylation. *EMBO J.* 11:1773–1784.

Vergés, E., N. Colomina, E. Garí, C. Gallego, and M. Aldea. 2007. Cyclin Cln3 is retained at the ER and released by the J chaperone Ydj1 in late G1 to trigger cell cycle entry. *Mol. Cell*. 26:649–662. http://dx.doi.org/10.1016/j.molcel.2007.04.023

Villén, J., and S.P. Gygi. 2008. The SCX/IMAC enrichment approach for global phosphorylation analysis by mass spectrometry. *Nat. Protoc.* 3:1630–1638. http://dx.doi.org/10.1038/nprot.2008.150

Voth, W.P., Y. Yu, S. Takahata, K.L. Kretschmann, J.D. Lieb, R.L. Parker, B. Milash, and D.J. Stillman. 2007. Forkhead proteins control the outcome of transcription factor binding by antiactivation. *EMBO J.* 26:4324–4334. http://dx.doi.org/10.1038/sj.emboj.7601859

Weiss, E.L., C. Kurischko, C. Zhang, K. Shokat, D.G. Drubin, and F.C. Luca. 2002. The *Saccharomyces cerevisiae* Mob2p–Cbk1p kinase complex promotes polarized growth and acts with the mitotic exit network to facilitate daughter cell–specific localization of Ace2p transcription factor. *J. Cell Biol.* 158:885–900. http://dx.doi.org/10.1083/jcb.200203094

Yaglom, J.A., A.L. Goldberg, D. Finley, and M.Y. Sherman. 1996. The molecular chaperone Ydj1 is required for the p34CDC28-dependent phosphorylation of the cyclin Cln3 that signals its degradation. *Mol. Cell. Biol.* 16:3679–3684.

Young, P.G., and P.A. Fantes. 1987. *Schizosaccharomyces pombe* mutants affected in their division response to starvation. *J. Cell Sci.* 88:295–304.

Yu, H.G., and D. Koshland. 2007. The Aurora kinase Ipl1 maintains the centromeric localization of PP2A to protect cohesin during meiosis. *J. Cell Biol.* 176:911–918. http://dx.doi.org/10.1083/jcb.200609153

Zhao, Y., G. Boguslawski, R.S. Zitomer, and A.A. DePaoli-Roach. 1997. *Saccharomyces cerevisiae* homologs of mammalian B and B' subunits of protein phosphatase 2A direct the enzyme to distinct cellular functions. *J. Biol. Chem.* 272:8256–8262. http://dx.doi.org/10.1074/jbc.272.13.8256